Published in final edited form as:
Sci Signal. ; 6(293): ra83. doi:10.1126/scisignal.2004214.

The Transcription Factor CREB Enhances Interleukin-17A Production and Inflammation in a Mouse Model of Atherosclerosis

Sivareddy Kotla[1], **Nikhlesh K. Singh**[1], **Mark R. Heckle**[1], **Gabor J. Tigyi**[1], and **Gadiparthi N. Rao**[1,*]

[1]Department of Physiology, University of Tennessee Health Science Center, 894 Union Avenue, Memphis, TN 38163, USA

Abstract

It has been demonstrated that 15-lipoxygenase (15-LO) plays a role in atherogenesis, but the underlying mechanisms were unclear. Therefore, the purpose of the present study is to explore the mechanisms of 15-LO role in atherogenesis. 15(S)-hydroxyeicosatetraenoic acid [15(S)-HETE], the major 15-LO-dependent metabolite of arachidonic acid (AA), stimulated the production of reactive oxygen species (ROS) by monocytes through the xanthine oxidase–mediated activation of NADPH oxidase, which led to the Syk-, Pyk2-, mitogen-activated protein kinase (MAPK)–, and cyclic adenosine monophosphate response element–binding protein (CREB)–dependent production of the pro-inflammatory cytokine interleukin-17A (IL-17A). In addition, this pathway was required for the 15(S)-HETE–dependent migration and adhesion of monocytes to endothelial cells. Consistent with these observations, we found that peritoneal macrophages from ApoE$^{-/-}$ mice fed a high-fat diet (a mouse model of atherosclerosis) exhibited increased xanthine oxidase and NADPH oxidase activities, ROS production, phosphorylation of Syk, Pyk2, MAPK, and CREB, and enhanced IL-17A production compared to those from ApoE$^{-/-}$:12/15-LO$^{-/-}$ mice. These events correlated with increased lipid deposits and numbers of monocytes and macrophages in the aortic arches of these mice, which resulted in atherosclerotic plaque formation. Together, these observations suggest that 15(S)-HETE exacerbates atherogenesis by enhancing CREB-dependent IL-17A production.

INTRODUCTION

Cardiovascular diseases are the leading cause of death and disability in the world (1). Atherosclerosis, which is a chronic inflammatory disease, is the major cause of heart failure and stroke, and it accounts for most of the deaths caused by cardiovascular diseases (1, 2). Atherosclerosis is characterized by thickening of the arterial wall as a result of the accumulation of lipid-laden foam cells of macrophage and smooth muscle cell origin, as well as calcification (3). A large body of data shows that lipoxygenases (LOs), particularly 5- and 15-LOs, which are enzymes that catalyze diooxygenation of polyunsaturated fatty acids, play a role in the pathogenesis of this disease (4–7). One of the most explored and

*Corresponding author. rgadipar@uthsc.edu.

Author contributions: S.K. performed monocyte migration and adhesion assays, Western blotting, immunoprecipitations, ELISA, ROS measurements, RT-PCR, mouse feeding with a high-fat diet, and isolation of peritoneal macrophages; M.R.H. performed Western blotting and macrophage isolation; N.K.S. performed monocyte migration and adhesion assays, Western blotting, immunoprecipitations, ROS measurements, isolation of peritoneal macrophages, and immunofluorescence staining of aortic arch sections; G.J.T. participated in project discussions and wrote the manuscript; G.N.R. conceived the overall project, designed the experiments, interpreted the data, and wrote the manuscript.

Competing interests: The authors declare that they have no competing interests.

best appreciated mechanisms of the involvement of LOs in atherogenesisis the capacity of 15-LO to oxidize low-density lipoprotein (LDL) (8–11). LOs catalyze the stereospecific insertion of molecular oxygen into cis-polyunsaturated fatty acids, such as arachidonic acid (AA) and linoleic acid, which results in the formation of hydroperoxyeicosatetraenoic acids (HpETEs) and hydroperoxyoctadecadienoic acids (HpODEs), respectively (12, 13). HpETEs and HpODEs are then non-enzymatically converted to hydroxyeicosatetraenoic acids (HETEs) and hydroxyoctadecadienoic acids (HODEs), respectively. 15-LO1 and 15-LO2 catalyze the conversion of AA mainly to 15(S)-HpETE (14, 15), whereas the murine ortholog of 15-LO1, which is known as 12/15-LO, converts AA to 12(S)-HpETE and 15(S)-HpETE (13). Some studies have demonstrated that when exposed to AA, atherosclerotic arteries produce more 15-HETE than do normal arteries (16, 17). Furthermore, many of the risk factors for cardiovascular disease, such as hypercholesterolemia, diabetes, obesity, and smoking, are associated with the increased abundance or activity of 12/15-LO (18–22). In addition, HETEs are pro-oxidants (that is, they induce oxidative stress) (23), and many reports showed that oxidative stress is linked to the pathogenesis of various disorders, including cardiovascular diseases, cancer, and rheumatoid arthritis (24, 25). Despite this, little is known regarding the role of HETEs in atherosclerosis other than the fact that 15-LO mediates the oxidation of LDL (9–11).

Because the migration of monocytes and macrophages to sites of vascular injury and their adhesion to endothelium are considered to be the hallmarks of the initiation of atherogenesis (1), we hypothesized that 15(S)-HETE, the major 15-LO–dependent product of AA, enhanced the migration and adhesion of monocytes and macrophages to endothelium, thereby provoking inflammation. Here, we found that 15(S)-HETE enhanced the migration and adhesion of macrophages to monolayers of endothelial cells in vitro. In addition, we showed that 15(S)-HETE stimulated the production of reactive oxygen species (ROS) by activating the xanthine oxidase–dependent NADPH (nicotinamide adenine dinucleotide phosphate) oxidase, which led to stimulation of the transcription factor CREB [cyclic adenosine monophosphate (cAMP) response element (CRE)–binding protein] and production of the pro-inflammatory cytokine interleukin-17A (IL-17A), which facilitated monocyte and macrophage migration and adhesion. Stimulation of CREB depended on the activities of the nonreceptor tyrosine kinases Syk and Pyk2, as well as the mitogen-activated protein kinases (MAPKs). Furthermore, peritoneal macrophages isolated from mice deficient in apolipoprotein E ($ApoE^{-/-}$ mice) that were fed a high-fat diet (a mouse model of atherosclerosis) exhibited substantially increased activities of xanthine oxidase and NADPH oxidase, production of ROS, phosphorylation of Syk, Pyk2, MAPK, and CREB, and production of IL-17A compared to those isolated from $ApoE^{-/-}$:12/15-$LO^{-/-}$ mice fed a high-fat diet. These observations also correlated with increased amounts of ROS, lipid deposits, numbers of monocytes and macrophages, IL-17A production, and plaque formation in the aortic arches of $ApoE^{-/-}$ mice compared to those of $ApoE^{-/-}$:12/15-$LO^{-/-}$ mice fed a high-fat diet, which is suggestive of a crucial role for 12/15-LO in the development of high-fat diet–induced oxidant stress and inflammation. These findings indicate that 12/15-LO plays a role in atherogenesis by enhancing CREB-dependent IL-17A production.

RESULTS

15(S)-HETE stimulates the migration of THP1 cells and their adhesion to endothelial cells in a ROS-dependent manner

Inflammation is considered to be an underlying factor for atherogenesis (26, 27). In addition, a role for LOs in atherogenesis and inflammation has been demonstrated (4–7, 21). However, the mechanisms by which LOs influence atherogenesis are not clear other than that 15-LO oxidizes LDL (9–11). To understand the role of LOs in atherogenesis, we

studied the effects of 5-, 12-, and 15(S)-HETE, which are derived by cleavage of AA by 5-LO, 12-LO, and 15-LO, respectively, on the migration and adhesion of monocytes. Of all the HETEs tested, 15(S)-HETE was the most potent in stimulating both the migration of THP1 cells (a human monocytic cell line) and their adhesion to a monolayer of human umbilical vein endothelial cells (HUVECs) (Fig. 1, A and B). 15(S)-HETE was more potent than 15(R)-HETE in stimulating both the migration and adhesion of THP1 cells (Fig. 1, C and D), which suggests that these effects are specific to 15-LO metabolites of AA. Analysis of the dose-response effect of 15(S)-HETE showed that maximal effects on THP1 cell migration and adhesion occurred at 0.1 μM 15(S)-HETE (Fig. 1, E and F).

To understand the mechanisms underlying the 15(S)-HETE–dependent migration and adhesion of THP1 cells, we tested its effects on ROS production. 15(S)-HETE stimulated ROS production in a time-dependent manner, with a maximal four-fold increase in ROS generation 1 hour after treatment (Fig. 2A). A convincing body of evidence suggests that NADPH oxidase and xanthine oxidase are the major producers of ROS in most cell types (25, 28, 29). Therefore, to find the source of 15(S)-HETE-induced ROS, we tested the roles of NADPH oxidase and xanthine oxidase in THP1 cells. 15(S)-HETE stimulated the activities of both NADPH oxidase and xanthine oxidase in a time-dependent manner with a maximal three- to five-fold increase 30 min after treatment (Fig. 2, B and C). In addition, we found that the NAPDH oxidase inhibitors apocyanin and diphenyleneiodonium (DPI) (30), as well as the xanthine oxidase inhibitor allopurinol (30), substantially reduced the extent of 15(S)-HETE–dependent ROS production (Fig. 2D).

To confirm these findings, we used an antisense oligonucleotide (ASO) approach. Depletion of either p47Phox, a component of NADPH oxidase (28), or xanthine oxidase substantially attenuated 15(S)-HETE–dependent ROS production (Fig. 2E) in THP1 cells. Inhibition or depletion of NADPH oxidase or xanthine oxidase also blocked the 15(S)-HETE–dependent migration and adhesion of THP1 cells (Fig. 2, F and G). Because inhibition or depletion of NADPH oxidase and xanthine oxidase similarly attenuated 15(S)-HETE–dependent ROS production, we next asked whether there was any interaction between these oxidases. Inhibition of NADPH oxidase activity or depletion of NADPH oxidase protein by pharmacological or ASO-based approaches, respectively, had minor effects on 15(S)-HETE–dependent xanthine oxidase activity (Fig. 2H). On the other hand, inhibition of xanthine oxidase activity or depletion of xanthine oxidase protein by pharmacological or ASO-based approaches, respectively, substantially attenuated 15(S)-HETE–dependent NADPH oxidase activity (Fig. 2I), similarly to that of specific NADPH oxidase inhibitors, suggesting that 15(S)-HETE–stimulated NADPH oxidase activity and ROS production depend on xanthine oxidase activity.

We also tested the role of xanthine oxidase in the phosphorylation of the NADPH oxidase component p47Phox (25, 28). We found that 15(S)-HETE stimulated the phosphorylation of p47Phox in a time-dependent manner (Fig. 2J), and knockdown of xanthine oxidase abundance by ASO substantially inhibited this effect (Fig. 2J). These findings suggest that 15(S)-HETE stimulated NADPH oxidase activity in a xanthine oxidase–dependent manner, leading to the production of ROS. To obtain additional evidence for these effects of 15(S)-HETE, we also tested its effects on the activities of NADPH oxidase and xanthine oxidase and ROS production in mouse primary macrophages. 15(S)-HETE stimulated NADPH oxidase and xanthine oxidase activities, as well as ROS production, in a time-dependent manner, with maximal increases after 1 hour of treatment (Fig. 3, A to C). Consistent with these effects, 15(S)-HETE also induced the migration and adhesion of these cells to a monolayer of mouse endothelial cells (Fig. 3, D and E).

15(S)-HETE–stimulated migration and adhesion of THP1 cells requires ROS-dependent activation of Syk and Pyk2

ROS act as intracellular signals primarily through their capacity to inhibit protein tyrosine phosphatases (PTPs), thereby tilting the balance of the system towards the activation of protein tyrosine kinases (PTKs) (31, 32). Having found that 15(S)-HETE stimulated ROS production, we next asked whether ROS led to the activation of any nonreceptor tyrosine kinases. We tested the effect of 15(S)-HETE on the activation of three nonreceptor tyrosine kinases, Src, Syk, and Pyk2. Although 15(S)-HETE caused only a marginal increase in the tyrosine phosphorylation of Src, it stimulated the tyrosine phosphorylation of both Syk and Pyk2 in a time-dependent manner, with near-maximal increases in phosphorylation 1 hour after treatment (Fig. 4A). To test the roles of Syk and Pyk2 in the 15(S)-HETE–dependent migration and adhesion of THP1 cells, we used a combination of pharmacological and genetic approaches. We found that BAY61-3606 and PF431396, specific inhibitors of Syk (33) and Pyk2 (34), respectively, inhibited 15(S)-HETE–stimulated migration and adhesion of THP1 cells (Fig. 4B). Similarly, ASO-mediated reduction in the abundance of Syk or Pyk2 also reduced the 15(S)-HETE–dependent migration and adhesion of THP1 cells (Fig. 4C).

To understand the mechanisms by which Syk and Pyk2 were activated by 15(S)-HETE, we tested the role of ROS. Inhibition or depletion of either NADPH oxidase or xanthine oxidase attenuated the 15(S)-HETE–dependent phosphorylation of Syk and Pyk2 (Fig. 4D). Because, 15(S)-HETE activated both Syk and Pyk2 with similar time courses, we asked whether there was any interaction between these two kinases. Inhibition or depletion of Syk blocked the 15(S)-HETE–dependent phosphorylation of Pyk2 (Fig. 4E).Conversely, inhibition or depletion of Pyk2 substantially inhibited the phosphorylation of Syk (Fig. 4E), which suggested that each kinase depended on the other for activation.

Based on these observations, we performed coimmunoprecipitation experiments to determine whether Syk and Pyk2 interacted with each other. We found that both Syk and Pyk2 physically associated with each other in THP1 cells, and that this interaction was enhanced in response to 15(S)-HETE (Fig. 4F). To explore potential signaling events downstream of the 15(S)-HETE-dependent activation of Syk and Pyk2, we tested the stimulation of MAPKs. 15(S)-HETE induced the phosphorylation of extracellular signal–regulated kinases 1 and 2 (ERK1/2), c-Jun N-terminal kinases 1 and 3 (JNK1/3), and p38 in a time-dependent manner, with maximal responses 1 hour after treatment (Fig. 5A). In addition, PD098059, SP600125 and SB203580, which specifically inhibit MEK1/2 (kinases that activate ERK1/2), JNK1/2, and p38, respectively (35), inhibited 15(S)-HETE–stimulated THP1 cell migration and adhesion (Fig. 5B). Furthermore, inhibition or depletion of NADPH oxidase, xanthine oxidase, Syk, or Pyk2 blocked 15(S)-HETE–dependent phosphorylation of ERK1/2, JNK1/3, and p38 (Fig. 5, C and D). These findings revealed that 15(S)-HETE stimulated the activation of ERK1/2, JNK1/3, and p38 in a manner dependent on xanthine oxidase, NADPH oxidase, Syk, and Pyk2.

15(S)-HETE–stimulated migration and adhesion of THP1 cells requires ROS, Syk, Pyk2, and MAPK-dependent activation of CREB

Having observed that 15(S)-HETE stimulated MAPK activation, we next asked whether these responses led to the activation of transcription factors. We and others showed that MAPKs mediate the activation of ATF2 (activating transcription factor 2) and CREB during 15(S)-HETE–stimulated migration of endothelial cells and vascular smooth muscle cells (15, 36). Therefore, we tested the effect of 15(S)-HETE on ATF2 and CREB activation in THP1 cells. We found that whereas 15(S)-HETE had no effect on ATF2 phosphorylation, it stimulated CREB phosphorylation in a time-dependent manner with a maximal response

after 1 hour of treatment (Fig. 6A). ASO-mediated knockdown of CREB inhibited the 15(S)-HETE–stimulated migration and adhesion of THP1 cells (Fig. 6B). To elucidate the mechanisms underlying 15(S)-HETE–dependent CREB activation, we tested the roles of NADPH oxidase, xanthine oxidase, Syk, Pyk2, and the MAPKs. Depletion of NADPH oxidase, xanthine oxidase, Syk, or Pyk2, or pharmacological inhibition of MAPKs attenuated the 15(S)-HETE–dependent phosphorylation of CREB (Fig. 6, C to E).

15(S)-HETE–stimulated migration and adhesion of THP1 cells requires ROS-, Syk-, Pyk2-, MAPK-, and CREB-dependent production of IL-17A

We next studied the effects of 15(S)-HETE on the production of the proinflammatory cytokines IL-11, IL-17A, and tumor necrosis factor α (TNF-α) by THP1 cells. Whereas 15(S)-HETE reduced the abundances of both *IL-11* and *TNF-α* mRNAs in THP1 cells, it increased *IL-17A* mRNA abundance in a time-dependent manner, with a maximal effect after 2 hours of treatment (Fig. 7A). Because 15(S)-HETE increased the abundance of *IL-17A* mRNA, we next examined its effects on IL-17A protein abundance, and found that it stimulated maximal IL-17A protein production after 2 hours of treatment (Fig. 7B). IL-17A stimulated the migration and adhesion of THP1 cells in a dose-dependent manner, with a maximum response at a concentration of 20 ng/ml (Fig. 7C). Furthermore, neutralizing anti–IL-17A antibodies blocked the IL-17A–dependent, as well as the 15(S)-HETE–dependent, migration and adhesion of THP1 cells (Fig. 7D). ASO-mediated depletion of NADPH oxidase, xanthine oxidase, Syk, Pyk2, or CREB, and pharmacological inhibition of MAPKs attenuated the 15(S)-HETE–dependent production of IL-17A (Fig. 7, E to H). These observations suggest that 15(S)-HETE stimulates the migration and adhesion of THP1 cells through the xanthine oxidase–dependent NADPH oxidase–mediated production of ROS, which leads to the activation of a signaling axis consisting of Syk, Pyk2, and various MAPKs, which culminates in activation of the transcription factor CREB and the production of IL-17A.

12/15-LO mediates the production of IL-17A in mice fed a high-fat diet

Apolipoprotein E-deficient ($ApoE^{-/-}$) mice develop atherogenesis spontaneously and so these mice were used as a model to study the pathogenesis of atherosclerosis (2). Previous studies have shown that deletion of 12/15-LO in $ApoE^{-/-}$ mice attenuates high-fat diet-induced atherogenesis (5, 10). Therefore, to explore the pathophysiological importance of these findings, we used both $ApoE^{-/-}$ and $ApoE^{-/-}$:12/15-$LO^{-/-}$ mice. After feeding $ApoE^{-/-}$ mice and $ApoE^{-/-}$:12/15-$LO^{-/-}$ mice with a high-fat diet for 8 weeks, we studied the signaling events that we characterized earlier in monocytes and macrophages. We found that macrophages from $ApoE^{-/-}$:12/15-$LO^{-/-}$ mice exhibited substantially reduced migration and adhesion capacities compared to those of $ApoE^{-/-}$ mice, as well as demonstrating comparatively reduced NADPH oxidase and xanthine oxidase activities, ROS production, Syk, Pyk2, MAPK, and CREB phosphorylation, and IL-17A production (Fig. 8, A to C). Furthermore, the plasma concentration of IL-17A was substantially lower in $ApoE^{-/-}$:12/15-$LO^{-/-}$ mice than in $ApoE^{-/-}$ mice (Fig. 8D). In contrast, the concentration of the anti-inflammatory cytokine IL-10 was substantially greater in $ApoE^{-/-}$:12/15-$LO^{-/-}$ mice than in $ApoE^{-/-}$ mice (Fig. 8D). Thus, these in vivo findings suggest that 12/15-LO plays a role in enhancing the inflammation elicited by the xanthine oxidase–dependent and NADPH oxidase–dependent ROS production that leads to Syk-Pyk2-MAPK-mediated CREB activation and IL-17A production. These observations also suggest that 12/15-LO increases the cellular oxidant state of inflammatory cells, particularly monocytes and macrophages, in response to the cardiovascular risk factors of high-fat diet and increased caloric intake.

To correlate these observations with plaque formation, we isolated the aortic arches from $ApoE^{-/-}$ mice and $ApoE^{-/-}$:12/15-$LO^{-/-}$ mice that were fed a high-fat diet for 8 weeks, and examined them for ROS production, lipid deposits, and numbers of monocytes and macrophages, as well as for IL-17A production. We observed increased amounts of ROS (both superoxide anion and H_2O_2), lipid deposits (by Oil Red O staining), and numbers of monocytes and macrophages in the aortic arches of $ApoE^{-/-}$ mice compared to those of $ApoE^{-/-}$:12/15-$LO^{-/-}$ mice (Fig. 8, E to H). In addition, immunofluorescence staining showed that the aortic arches of $ApoE^{-/-}$ mice exhibited increased abundance of IL-17A compared to those of $ApoE^{-/-}$:12/15-$LO^{-/-}$ mice (Fig. 8I). Similarly, double immunofluorescence staining for the macrophage marker Mac-3 and IL-17A revealed that there was an increased number of IL-17A–producing macrophages in the aortic arches of $ApoE^{-/-}$ mice compared to those of $ApoE^{-/-}$:12/15-$LO^{-/-}$ mice fed a high-fat diet (Fig. 8I).

DISCUSSION

The presence of abnormal amounts of LDL represents a risk factor for cardiovascular diseases (8, 37). The major mechanism underlying the role of the oxidative modification of LDL in atherosclerosis is its uptake and retention by macrophages, which then transform into foam cells and accumulate in the arterial wall, resulting in increased thickness and hardening (1, 26, 27). The gradual accumulation of lipid-laden foam cells leads to plaque formation. Whereas the progression of the plaque eventually leads to occlusion of the artery, unstable plaques can also rupture and expose their thrombogenic matrix to blood, which leads to the formation of thrombo-embolic occlusions (37). Many reports showed that 15-LO1 and its murine ortholog 12/15-LO play a role in atherogenesis by mediating the oxidation of LDL (4–7, 9–11). Although the mechanisms by which 15-LO1 modifies LDL are still unclear, some reports showed that upon exposure to AA, atherosclerotic arteries, liver, or macrophages *in vivo*, *ex vivo* or *in vitro* generate 15-HETE to sub-micromolar concentrations (16, 17, 38, 39), which raises the possibility that this lipid mediator might have some influence in atherogenesis. Indeed, 15-HpETE, the peroxide form of 15-HETE, is capable of enhancing the oxidation of LDL in the presence of catalytic amounts of copper (23).

Because HpETEs are mostly unstable, we asked whether their relatively stable form, 15(S)-HETE, influences the atherogenic process. We previously showed that 15(S)-HETE enhances vascular wall remodeling in response to injury (14) and increases angiogenesis in response to ischemia (30). Having observed that 15(S)-HETE enhanced the migration of endothelial cells and smooth muscle cells, we reasoned that it might also promote the migration of monocytes and macrophages as well as their adhesion to endothelium, thereby influencing atherogenesis. Here, we found that 15(S)-HETE stimulated monocyte migration and adhesion to endothelium. Oxidative stress plays a crucial role in vascular diseases (24, 28). Because some reports showed that 15-HpETE promotes oxidative stress and enhances the oxidation of LDL in the presence of copper (23), we asked whether 15(S)-HETE had any role in producing ROS. We found that 15(S)-HETE enhanced ROS production in a time-dependent manner, and that this effect depended on the activities of both xanthine oxidase and NADPH oxidase.

We also showed that 15(S)-HETE–stimulated NADPH oxidase activation depended on xanthine oxidase activity. A large body of evidence suggests that NADPH oxidase is the major producer of ROS in vascular cells and in other cell types (25, 28). Early studies showed that xanthine oxidase plays a role in tissue reperfusion injury (29); however, to our knowledge, the possibility of there being an interaction between these two unrelated oxidases has not been examined before. Because allopurinol, a competitive inhibitor of xanthine oxidase (33), or knockdown of xanthine oxidase abundance with a specific ASO

blocked the 15(S)-HETE–dependent phosphorylation of p47Phox, a regulatory component of NADPH oxidase (29), it is likely that xanthine oxidase plays a role in the activation of NADPH oxidase. Furthermore, phosphorylation of p47phox is required for its membrane translocation where it forms a complex with Nox to assemble the active NADPH oxidase (25, 29). Thus, our findings uncover a potentially important mechanism by which xanthine oxidase and NADPH oxidase interact to stimulate the production of ROS in response to 15(S)-HETE.

Previous studies showed that oxidants, such as H_2O_2, inhibit protein tyrosine phosphatases (PTPs) and thereby enhance the phosphorylation of receptor and nonreceptor tyrosine kinases, causing their activation (31, 32). Here, we provide evidence that 15(S)-HETE stimulated the tyrosine phosphorylation of Syk and Pyk2 through the xanthine oxidase– and NADPH oxidase–dependent production of ROS that in turn was required for the migration of THP1 cells and their adhesion to a HUVEC monolayer. Furthermore, Syk and Pyk2 mutually depended on each other for their phosphorylation, because inhibition of either kinase blocked the phosphorylation of the other. In support of this mechanism, we observed that a physical interaction between Syk and Pyk2 was enhanced in response to 15(S)-HETE. One possible explanation for the mutually dependent phosphorylation of Syk and Pyk2 might be a result of their association with a PTP. Inhibition of the associated PTP may lead to the phosphorylation and activation of one of these kinases acutely, which in turn, might have a priming effect on the phosphorylation of the other with a feed-forward mechanism.

Although a role for Syk in inflammation is not well-established, the involvement of Pyk2 in inflammation and atherogenesis has been reported (40, 41). In addition, both Syk and Pyk2 play a role in vascular wall remodeling in response to injury (42, 43). Here, we showed that both Syk and Pyk2 interacted with each other and mediated monocyte migration. Previously, we showed that 15(S)-HETE activates MAPKs in endothelial cells and vascular smooth muscle cells to mediate their migration (15, 30). Consistent with these observations, we found that 15(S)-HETE also stimulated the activation of ERK1/2, JNK1/3, and p38 in THP1 cells to mediate their migration and adhesion. In addition, the 15(S)-HETE–dependent activation of MAPK signaling required the activation of xanthine oxidase, NADPH oxidase, Syk, and Pyk2.

Many reports have shown that Src and Pyk2 mediate MAPK activation in response to external cues (31, 32, 44). We showed that by phosphorylating and activating CREB, MAPKs modulate the migration of vascular smooth muscle cells in response to 15(S)-HETE (15). Here, we also found that 15(S)-HETE activated CREB, and that stimulation of CREB activity was required for the migration of THP1 cells and for their adhesion to endothelial cells. Furthermore, the 15(S)-HETE–dependent activation of CREB required the stimulation of MAPK signaling downstream of xanthine oxidase, NADPH oxidase, Syk, and Pyk2. Studies indicate that CREB plays a role in the hormonal regulation of cell metabolism, neuronal plasticity, memory, and cell survival (45, 46). Our findings showed that in monocytes, CREB enhanced the production of proinflammatory cytokines, such as IL-17A, revealing a possible role for CREB in mediating inflammation. Furthermore, the blockade of 15(S)-HETE–dependent migration and adhesion of THP1 cells by neutralizing anti–IL-17A antibodies suggests that IL-17A mediates the inflammatory effects of CREB.

The adhesion of THP1 cells to a monolayer of HUVECs may require the availability of adhesion molecules. Studies showed that the LO-dependent products derived from linoleic acid, such as 13-HpODE, stimulate the production of vascular cell adhesion molecule (VCAM) by HAECs (human aortic endothelial cells) (47). Based on this information, we hypothesize that 15(S)-HETE might stimulate the production of cell adhesion molecules,

such as VCAM, by HUVECs, which could facilitate the adhesion of monocytes and macrophages, and that this effect may also depend on IL-17A.

Many studies have shown that deletion of the gene encoding 12/15-LO results in decreased atherosclerosis in ApoE$^{-/-}$ mice fed a high-fat or Western diet, which suggests a role for 12/15-LO in atherogenesis. In addition, it was reported that macrophages expressing 12/15-LO contribute to atherogenesis (48). However, the protective role of loss of 12/15-LO on atherosclerosis was attributed to the involvement of 12/15-LO in LDL oxidation. Here, we observed that peritoneal macrophages from ApoE$^{-/-}$ mice fed a high-fat diet exhibited substantially increased xanthine oxidase and NADPH oxidase activities, produced more ROS, had increased phosphorylation and activation of Syk, Pyk2, MAPK, and CREB, and produced more IL-17A than did ApoE$^{-/-}$:12/15-LO$^{-/-}$ mice fed a high-fat diet. These observations suggest that 12/15-LO plays a critical role in ROS production, and that this response depends on the activities of xanthine oxidase and NADPH oxidase.

A number of studies have shown that IL-17A plays a role in vascular inflammation and atherogenesis (49, 50); however, some reports indicate that IL-17A alone may not be sufficient to account for aortic plaque burden (51). Because loss of 12/15-LO in mice fed a high-fat diet reduced the production of IL-17A, we propose that 12/15-LO plays a role in high-fat diet–induced IL-17A production in ApoE$^{-/-}$ mice. In addition, we found that the increased abundance of IL-17A correlated with the number of macrophages in the lesion area, which was substantially higher in ApoE−/− mice than in ApoE$^{-/-}$:12/15-LO$^{-/-}$ mice. This suggests that the 12/15-LO–12/15(S)-HETE axis plays a role in stimulating IL-17A production in macrophages, causing their migration in an autocrine manner. Furthermore, given the known role for IL-17A in promoting inflammation (49–51), it is tempting to suggest that 12/15-LO, through its regulatory effect on IL-17A production, plays a major role in atherogenic inflammation. In this context, we should also point out that a report showed that 12/15-LO mediates inflammation in adipose tissue (21). Other reports showed that the cytokine IL-8 stimulates the production of 15-HETE by neutrophils (52). Here, we showed that 12/15-LO and 15(S)-HETE both played a role in increasing the production of IL-17A. Based on these observations, we suggest that there is a feed-forward circuitry between 12/15-LO and cytokine regulation in the modulation of atherogenic inflammation. Because 15(S)-HETE stimulates the xanthine oxidase– and NADPH oxidase–dependent generation of ROS, it is possible that this mechanism, activated by 12/15-LO, mediates the oxidation of LDL in atherogenesis. Based on these findings, we suggest that 12/15-LO plays an important role in the generation of oxidative stress and inflammation in response to a high-fat or Western diet, and thereby might promote the development of atherosclerotic lesions. Together, these findings suggest that 12/15-LO appears to be an upstream modulator of atherogenesis and that it might be a target for drug development.

MATERIALS AND METHODS

Reagents

Anti-pCREB (9198), anti-pERK1/2 (9101), anti-pJNK1/3 (9251), anti-pp38 MAPK (9215), anti-pPyk2 (3291), and anti-pSyk (2715) antibodies were purchased from Cell Signaling Technology. Anti-CD68 (SC-9139), anti-CREB (SC-58), anti-ERK2 (SC-154), anti–IL-17 (SC-374218), anti-JNK3 (SC-752), anti–Mac-3 (SC-19991), anti-p38 MAPK (SC-538), anti-p47Phox (SC-14015), anti-Syk (SC-573), anti-β-tubulin (SC-9104), and anti-XO (SC-20991) antibodies were obtained from Santa Cruz Biotechnology, Inc. Anti-Pyk2 (ab32571) and anti–CD-11b (ab8878) antibodies, as well as the IL-17–specific enzyme-linked immunosorbent assay (ELISA) kit (ab100702) were purchased from Abcam. 5(S)-HETE (34230), 12(S)-HETE (34570), 15(R)-HETE (34710), 15(S)-HETE (34720), and the xanthine oxidase kit (10010895) were obtained from Cayman Chemicals. The NADPH

oxidase kit (KA1663) was obtained from Abnova. Thioglycolate medium, brewer-modified (21176) was purchased from BD Biosciences. Apocynin (A10809) and allopurinol (A8003) were obtained from Sigma Aldrich Chemicals. Diphyneleneiodonium chloride (BML-CN240) and PD-098059 (BML-EI360) were purchased from Enzo Life Science. SP328007 and SB559389 were obtained from Calbiochem. The Lipofectin transfection reagent (15596018), CM-H2DCFDA (C6827), DHE (D11347), BCECF-AM (B1170), and TRIzol reagent were obtained from Invitrogen. Human recombinant IL-17 (317-ILB-050), IL-17–specific neutralizing antibody (AF-317-NA), and the IL-10 ELISA kit (M10000B) were obtained from R&D Systems. The ECL Western blotting detection reagents (RPN2106) were obtained from GE Health Care. The following phosphorothiolate-modified antisense oligonucleotides were synthesized by IDT: hControl ASO: 5′-GGGGGUTCTCTGCGTACGGTGCUAGU-3’; hp47Phox (NM_000265) ASO1: 5′-GGGCUCAGGGTCTTCCGTCUCGUC-3’; hp47Phox ASO2: 5′-GUUGGGCTCAGGGTCTTCCGUCUC-3’; hXO (NM_000379) ASO1: 5′-CCCAUCTCCTCCACAGCAUCCACC-3’; hXO ASO2: 5′-GCCUCCTCCCATTCTCTTCACUCG-3’; hSyk (NM_001174168) ASO1: 5′-CCCAUCCGCTCTCCTUUCUC-3’; hSyk ASO2: 5′-CUUCCCTGTCTTGTCUUUGU-3’; hSyk ASO3: 5′-UUCCCTGTCTTGTCTUUGUC-3’; hPyk2 (NM_173175) ASO1: 5′-GGCGGUTCTGCGTACGGTGCUAGU-3’; hPyk2 ASO2: 5′-GGUCUGTACTTAGGTCGGCUGGGC-3’; hPyk2 ASO3: 5′-CCUGUGTCCATAGCCCAGAGUACC-3’; hCREB (NM_004379) ASO1: 5′-CUCUGCTGGTTCTCGGCUCC-3’; hCREB ASO2: 5′-GUGGCAATCTGTGGCUGGGC-3’; and hCREB ASO3: ‘5-GCUGCTTCCCTGTTCUUCAU-3’. h, human.

Cell culture

THP1 cells, a human leukemic monocyte cell line, were purchased from the American Type Culture Collection (ATCC) and cultured in RPMI-1640 medium supplemented with 10% heat-inactivated fetal bovine serum (FBS), penicillin (50 U/ml), streptomycin (50 μg/ml), and 50 μM β-mercaptoethanol. HUVECs were obtained from Invitrogen and were cultured in Medium 200 with low serum growth supplements (LSGS), containing gentamycin (10 μg/ml) and amphotericin B (0.25 μg/ml). Mouse pancreatic endothelial cells were obtained from ATCC and were maintained in DMEM-F12 medium supplemented with 10% FBS, penicillin (50 U/ml), and streptomycin (50 μg/ml). All cell cultures were maintained in a humidified 95% air and 5% CO_2 atmosphere at 37°C.

Cell migration assays

A modified Boyden chamber method was used to measure cell migration (15). THP1 cells were growth-arrested overnight in serum-free RPMI-1640 medium. Cells were resuspended in serum-free medium and plated on Matrigel-coated cell culture inserts at 5×10^4 cells/insert. 15(S)-HETE was added to a final concentration of 0.1 μM to both the upper and lower chambers, and the cells were incubated for 8 hours at 37°C. The inserts were then lifted, non-migrated cells on the upper surface of the membrane were removed with a cotton swab, and the membrane was then fixed in methanol and stained with DAPI (4’,6-diamidino-2-phenylindole) to visualize nuclei. Whenever ASOs were used, cells were transfected first with the indicated ASOs for 6 hours in serum-free medium before being maintained in complete medium for 36 hours and then being subjected to growth-arrest and migration. Whenever inhibitors were used, cells were incubated first with the indicated inhibitor for 30 min. The DAPI-positive cells were counted under an inverted microscope (Carl Zeiss AxioVision AX10) and the extent of migration was expressed as the number of cells per field of view.

Cell adhesion assays

The adhesion of THP1 cells to HUVECs was measured with a fluorometric method (53). Briefly, quiescent THP1 cells were left untreated or were treated with 0.1 μM 15(S)-HETE for 1 hour at 37°C and then were labeled with 10 μM BCECF-AM [2',7'-bis-(2-carboxyethyl)-5(and-6)-carboxyfluorescein-acetoxymethyl) in serum-free medium for 30 min. The labeled cells were plated on a quiescent monolayer of HUVECs at 8×10^4 cells/well, and were incubated for a further 2 hours, after which, any nonadherent THP1 cells were washed out with phosphate-buffered saline (PBS). The adherent BCECF-AM–labeled THP1 cells were then lysed in 0.2 ml of 0.1 M Tris-HCl containing 0.1% Triton X-100, and the fluorescence intensity was measured in a Spectra Max Gemini XS Spectroflurometer (Molecular Devices) with excitation at 485 nm and emission at 535 nm. Cell adhesion was expressed as relative fluorescence units.

ELISA

The concentrations of IL-10 and IL-17 in plasma from mice were measured with specific ELISA kits according to the manufacturers' instructions (R&D systems and Abcam, respectively).

ROS detection

Intracellular ROS generation was measured with membrane-permeable 5-(6)-chloromethyl-2',7'-dichlorodihydrofluorescein diacetate (CM-H_2DCFDA), as described previously (54). After the treatments indicated in the figure legends, THP1 cells were incubated with 10 μM CM-H_2DCFDA for 30 min, washed with PBS, and resuspended in serum-free medium. The fluorescence intensities of the resuspended cells were measured in a Spectra Max Gemini XS Spectroflurometer (Molecular Devices) with excitation at 485 nm and emission at 535 nm. To measure ROS concentrations in mouse arteries, aortic arch sections of $ApoE^{-/-}$ mice and $ApoE^{-/-}$: 12/15-$LO^{-/-}$ mice fed a high-fat diet were stained with the dyes DHE (dihydroethidium) and CM-H_2DCFDA to detect superoxide anions and H_2O_2, respectively (55), and fluorescence intensities were measured with Nikon NIS-Elements software version AR 3.1. ROS production was expressed as relative fluorescence units.

RT-PCR

Total cellular RNA was extracted from THP1 cells with TRIzol reagent according to the manufacturer's instructions. Reverse transcription was performed with a High Capacity cDNA Reverse Transcription kit (Applied Biosystems). Complementary DNA (cDNA) was then used as a template for amplification by polymerase chain reaction (PCR) with the following primers: human *IL-11* (NM_000641): forward: 5′-CTGAGCCTGTGGCCAGATACA-3′; reverse: 5′-CTCCAGGGTCTTCAGGGAAGA-3′; human *TNF-α* (NM_000594): forward: 5′-CAGAGGGCCTGTACCTCATC-3′; reverse: 5′-GGAAGACCCCTCCCAGATAG-3′; human *IL-17A* (NM_002190): forward: 5′-GCAATGAGGACCCTGAGAGA-3′; reverse: 5′-CCCACGGACACCAGTATCTT-3′; human *β-actin* (NM_001101) forward: 5′-AGCCATGTACGTTGCTAT-3′; reverse: 5′-GATGTCCACGTCACACTTCA-3′. The amplification was performed with a Gene Amp PCR System 2400 (Applied Biosystems). The amplified PCR products were separated on 1.5% (w/v) agarose gels, stained with ethidium bromide, and images were captured with a Kodak In-Vivo Imaging System.

Western blotting

Whole-cell lysates containing equal amounts of protein were resolved by electrophoresis on 0.1% (W/V) SDS and 10% (W/V) polyacrylamide gels. The proteins were transferred

electrophoretically to a nitrocellulose membrane. After blocking in either 5% (W/V) nonfat dry milk or 5% (W/V) bovine serum albumin (BSA), the membrane was incubated with the appropriate primary antibodies followed by incubation with horseradish peroxidase (HRP)-conjugated secondary antibodies. The antigen-antibody complexes were detected with the Enhanced Chemiluminescence detection reagent kit (GE Health Care).

Measurement of NADPH oxidase and xanthine oxidase activities

NADPH oxidase and xanthine oxidase activities were measured with kits according to the manufacturers' instructions (Abnova and Cayman Chemicals, respectively).

Transfections

Cells were transfected with the indicated ASOs (100 nM) with Lipofectin transfection reagent for 6 hours according to the manufacturer's instructions. After transfection, cells were maintained in complete RPMI-1640 medium for 36 hours, and then were incubated with serum-free medium overnight before being used for experiments.

Isolation of peritoneal macrophages and collection of plasma and aortas from mice

ApoE−/− mice (stock number: 002052) were obtained from Jackson Laboratories (Bar Harbor, ME). ApoE$^{-/-}$ mice and ApoE$^{-/-}$:12/15-LO$^{-/-}$ mice (5) were bred and maintained according to guidelines of the Institutional Animal Care and Use Facility. All of the experiments involving mice were approved by the Animal Care and Use Committee of the University of Tennessee Health Science Center, Memphis, TN. Male 6-week-old ApoE$^{-/-}$ mice and ApoE$^{-/-}$:12/15-LO$^{-/-}$ mice were fed with a high-fat diet (protein: 15.2%; carbohydrate: 42.7%, and fat: 42%, Harlan Cat. No. TD.88137) for 8 weeks. To collect peritoneal macrophages, mice were injected intra peritoneally with 2 ml of autoclaved 4% thioglycolate. Four days later, the animals were anesthetized with ketamine and xylazine, and the peritoneal lavage was collected in RPMI-1640 medium. Cells were incubated at 3×10^5 cells/cm^2 in complete RPMI medium containing penicillin (50 μg/ml) and streptomycin (50 μg/ml). After 3 hours, floating cells (mostly red blood cells) were removed by washing with cold PBS. Adherent cells (macrophages) were used either for the extraction of total cellular protein for Western blotting analysis or to perform assays to measure migration, adhesion, ROS production, NADPH oxidase activity, or xanthine oxidase activity. Blood was drawn into 1.5-ml tubes containing anti-coagulant (20 μl of 0.5 M EDTA per tube) by cardiac puncture and centrifuged at 3500g for 5 min at 4°C to collect the plasma. The plasma was used to measure the concentrations of cytokines. The aortas and aortic arches were perfused with PBS, dissected, and fixed in OCT (optimal cutting temperature) compound.

Immunohistochemistry

Serial aortic arch sections (10 μm) were made with a Leica CM3050 S Cryostat machine, fixed in an equal volume of cold acetone and methanol for 10 min, permeabilized in 0.2% Triton-X 100 for 10 min, and blocked with 3% BSA for 30 min. The sections were then incubated with anti-Mac3 antibody (clone M3/84) primary antibody overnight at 4°C, which was followed by incubation with biotin-conjugated mouse anti-rat secondary antibody for 1 hour at room temperature. The sections were incubated with the ABC reagent for 30 min, developed with DAB reagent (Vector Laboratories), and counterstained with hematoxylin. The sections were observed with a Nikon Eclipse 50i microscope with 4×/0.10 or 10×/0.25 magnification, and images were captured with a Nikon Digital Sight DS-L1 camera.

Oil Red O staining

After fixing with 4% (v/v) paraformaldehyde, the aortic arch sections were stained with Oil Red O and counterstained with hematoxylin. Images were captured as described for immunohistochemistry.

Immunofluorescence staining

The aortic arch sections were fixed with acetone:methanol (1:1) for 10 min, permeabilized in 0.2% Triton X-100 for 10 min, blocked with 5% goat serum in 3% BSA for 1 hour, and incubated with rat anti–mouse CD11b and rabbit anti–mouse CD68 or rat anti–mouse Mac3 and mouse anti–human IL-17 antibodies (all at a 1:100 dilution) followed by incubation with Alexa Fluor 568–conjugated goat anti-rat and Alexa Fluor 488–conjugated goat anti-rabbit or Alexa Fluor 488–conjugated goat anti-rat and Alexa Fluor 568–conjugated goat anti-mouse secondary antibodies, respectively. The sections were observed with a Zeiss inverted microscope (Zeiss AxioObserver.Z1; type, LD plan-Neofluar; Magnification at 10X/NA 0.4 or 40X/NA 0.6), and the fluorescence images were captured with a Zeiss AxioCam MRm camera with the microscope operating and Image Analysis Software AxioVision 4.7.2 (Carl Zeiss Imaging Solutions GmbH). The fluorescence intensities were measured with Nikon NIS-Elements software version AR 3.1.

Statistical analysis

All the experiments were performed three times and data are presented as means ± the standard deviation (SD). Statistical differences between untreated and treated samples were analyzed with the Student t test; $P < 0.05$ was considered statistically significant. In the case of RT-PCR and Western blotting assays, histochemistry, immunohistochemistry, and immunofluorescence staining, one representative set of data is shown. In the case of experiments with mice, each group consists of 6 animals.

Acknowledgments

We are thankful to Dr. Jerry L. Nadler of Eastern Virginia Medical School for providing us ApoE$^{-/-}$:12/15-LO$^{-/-}$ mice.

Funding: This work was supported by grants HL064165 and HL074860 from the National Heart, Lung and Blood Institute of the National Institutes of Health (to G.N.R.).

REFERENCES AND NOTES

1. Hansson GK, Hermansson A. The immune system in atherosclerosis. Nat Immunol. 2011; 12:204–212. [PubMed: 21321594]
2. Libby P, Ridker PM, Hansson GK. Progress and challenges in translating the biology of atherosclerosis. Nature. 2011; 473:317–3253. [PubMed: 21593864]
3. Stary HC, Chandler AB, Dinsmore RE, Fuster V, Glagov S, Insull W Jr, Rosenfeld ME, Schwartz CJ, Wagner WD, Wissler RW. A definition of advanced types of atherosclerotic lesions and a histological classification of atherosclerosis. A report from the Committee on Vascular Lesions of the Council on Arteriosclerosis, American Heart Association. Circulation. 1995; 92:1355–1374. [PubMed: 7648691]
4. Sendobry SM, Cornicelli JA, Welch K, Bocan T, Tait B, Trivedi BK, Colbry N, Dyer RD, Feinmark SJ, Daugherty A. Attenuation of diet-induced atherosclerosis in rabbits with a highly selective 15-lipoxygenase inhibitor lacking significant antioxidant properties. Br J Pharmacol. 1997; 120:1199–1206. [PubMed: 9105693]
5. Cyrus T, Witztum JL, Rader DJ, Tangirala R, Fazio S, Linton MF, Funk CD. Disruption of the 12/15-lipoxygenase gene diminishes atherosclerosis in apo E-deficient mice. J Clin Invest. 1999; 103:1597–1604. [PubMed: 10359569]

6. Harats D, Shaish A, George J, Mulkins M, Kurihara H, Levkovitz H, Sigal E. Overexpression of 15-lipoxygenase in vascular endothelium accelerates early atherosclerosis in LDL receptor-deficient mice. Arterioscler Thromb Vasc Biol. 2000; 20:2100–2105. [PubMed: 10978255]
7. Mehrabian M, Allayee H, Wong J, Shi W, Wang XP, Shaposhnik Z, Funk CD, Lusis AJ. Identification of 5-lipoxygenase as a major gene contributing to atherosclerosis susceptibility in mice. Circ Res. 2002; 91:120–126. [PubMed: 12142344]
8. Ylä-Herttuala S, Palinski W, Rosenfeld ME, Parthasarathy S, Carew TE, Butler S, Witztum JL, Steinberg D. Evidence for the presence of oxidatively modified low density lipoprotein in atherosclerotic lesions of rabbit and man. J Clin Invest. 1989; 84:1086–1095. [PubMed: 2794046]
9. Ylä-Herttuala S, Luoma J, Viita H, Hiltunen T, Sisto T, Nikkari T. Transfer of 15-lipoxygenase gene into rabbit iliac arteries results in the appearance of oxidation-specific lipid-protein adducts characteristic of oxidized low density lipoprotein. J Clin Invest. 1995; 95:2692–2698. [PubMed: 7769108]
10. Cyrus T, Praticò D, Zhao L, Witztum JL, Rader DJ, Rokach J, FitzGerald GA, Funk CD. Absence of 12/15-lipoxygenase expression decreases lipid peroxidation and atherogenesis in apolipoprotein e-deficient mice. Circulation. 2001; 103:2277–2282. [PubMed: 11342477]
11. Benz DJ, Mol M, Ezaki M, Mori-Ito N, Zelán I, Miyanohara A, Friedmann T, Parthasarathy S, Steinberg D, Witztum JL. Enhanced levels of lipoperoxides in low density lipoprotein incubated with murine fibroblast expressing high levels of human 15-lipoxygenase. J Biol Chem. 1995; 270:5191–5197. [PubMed: 7890629]
12. Brash AR. Lipoxygenases: occurrence, functions, catalysis, and acquisition of substrate. J Biol Chem. 1999; 274:23679–23682. [PubMed: 10446122]
13. Kühn H, Barnett J, Grunberger D, Baecker P, Chow J, Nguyen B, Bursztyn-Pettegrew H, Chan H, Sigal E. Overexpression, purification and characterization of human recombinant 15-lipoxygenase. Biochim Biophys Acta. 1993; 1169:80–89. [PubMed: 8334154]
14. Potula HS, Wang D, Quyen DV, Singh NK, Kundumani-Sridharan V, Karpurapu M, Park EA, Glasgow WC, Rao GN. Src-dependent STAT-3-mediated expression of monocyte chemoattractant protein-1 is required for 15(S)-hydroxyeicosatetraenoic acid-induced vascular smooth muscle cell migration. J Biol Chem. 2009; 284:31142–31155. [PubMed: 19736311]
15. Chava KR, Karpurapu M, Wang D, Bhanoori M, Kundumani-Sridharan V, Zhang Q, Ichiki T, Glasgow WC, Rao GN. CREB-mediated IL-6 expression is required for 15(S)-hydroxyeicosatetraenoic acid-induced vascular smooth muscle cell migration. Arterioscler Thromb Vasc Biol. 2009; 29:809–815. [PubMed: 19342597]
16. Henriksson P, Hamberg M, Diczfalusy U. Formation of 15-HETE as a major hydroxyeicosatetraenoic acid in the atherosclerotic vessel wall. Biochim Biophys Acta. 1985; 834:272–274. [PubMed: 3995065]
17. Simon TC, Makheja AN, Bailey JM. Formation of 15-hydroxyeicosatetraenoic acid (15-HETE) as the predominant eicosanoid in aortas from Watanabe Heritable Hyperlipidemic and cholesterol-fed rabbits. Atherosclerosis. 1989; 75:31–38. [PubMed: 2495011]
18. Hiltunen T, Luoma J, Nikkari T, Ylä-Herttuala S. Induction of 15-lipoxygenase mRNA and protein in early atherosclerotic lesions. Circulation. 1995; 92:3297–3303. [PubMed: 7586317]
19. Aggarwal NT, Pfister SL, Campbell WB. Hypercholesterolemia enhances 15-lipoxygenase-mediated vasorelaxation and acetylcholine-induced hypotension. Arterioscler Thromb Vasc Biol. 2008; 28:2209–2215. [PubMed: 18832753]
20. Hatley ME, Srinivasan S, Reilly KB, Bolick DT, Hedrick CC. Increased production of 12/15 lipoxygenase eicosanoids accelerates monocyte/endothelial interactions in diabetic db/db mice. J Biol Chem. 2003; 278:25369–25375. [PubMed: 12734208]
21. Chakrabarti SK, Cole BK, Wen Y, Keller SR, Nadler JL. 12/15-lipoxygenase products induce inflammation and impair insulin signaling in 3T3-L1 adipocytes. Obesity. 2009; 17:1657–1663. [PubMed: 19521344]
22. Yoshida H, Sasaki K, Hirowatari Y, Kurosawa H, Sato N, Furutani N, Tada N. Increased serum iron may contribute to enhanced oxidation of low-density lipoprotein in smokers in part through changes in lipoxygenase and catalase. Clin Chim Acta. 2004; 345:161–170. [PubMed: 15193991]

23. O'Leary VJ, Darley-Usmar VM, Russell LJ, Stone D. Pro-oxidant effects of lipoxygenase-derived peroxides on the copper-initiated oxidation of low-density lipoprotein. Biochem J. 1992; 282:631–634. [PubMed: 1554346]
24. Leopold JA, Loscalzo J. Oxidative risk for atherothrombotic cardiovascular disease. Free Radic Biol Med. 2009; 47:1673–1706. [PubMed: 19751821]
25. Lambeth JD. Nox enzymes, ROS, and chronic disease: an example of antagonistic pleiotropy. Free Radic Biol Med. 2007; 43:332–347. [PubMed: 17602948]
26. Galkina E, Ley K. Immune and inflammatory mechanisms of atherosclerosis. Annu Rev Immunol. 2009; 27:165–197. [PubMed: 19302038]
27. Tabas I, Glass CK. Anti-inflammatory therapy in chronic disease: challenges and opportunities. Science. 2013; 339:166–172. [PubMed: 23307734]
28. Drummond GR, Selemidis S, Griendling KK, Sobey CG. Combating oxidative stress in vascular disease: NADPH oxidases as therapeutic targets. Nat Rev Drug Discov. 2011; 10:453–471. [PubMed: 21629295]
29. Berry CE, Hare JM. Xanthine oxidoreductase and cardiovascular disease: molecular mechanisms and pathophysiological implications. J Physiol. 2004; 555:589–606. [PubMed: 14694147]
30. Oeckler RA, Kaminski PM, Wolin MS. Stretch enhances contraction of bovine coronary arteries via an NAD(P)H oxidase-mediated activation of the extracellular signal-regulated kinase mitogen-activated protein kinase cascade. Circ Res. 2003; 92:23–31. [PubMed: 12522117]
31. Tonks NK. Redox redux: revisiting PTPs and the control of cell signaling. Cell. 2005; 121:667–670. [PubMed: 15935753]
32. Nakashima I, Takeda K, Kawamoto Y, Okuno Y, Kato M, Suzuki H. Redox control of catalytic activities of membrane-associated protein tyrosine kinases. Arch Biochem Biophys. 2005; 434:3–10. [PubMed: 15629102]
33. Yamamoto N, Takeshita K, Shichijo M, Kokubo T, Sato M, Nakashima K, Ishimori M, Nagai H, Li YF, Yura T, Bacon KB. The orally available spleen tyrosine kinase Inhibitor 2-[7-(3,4-dimethoxyphenyl)-imidazo[1,2-c]pyrimidin-5-ylamino]nicotinamide dihydrochloride (BAY 61–3606) blocks antigen-induced airway inflammation in rodents. J Pharmacol Exp Ther. 2003; 306:1174–1181. [PubMed: 12766258]
34. Buckbinder L, Crawford DT, Qi H, Ke HZ, Olson LM, Long KR, Bonnette PC, Baumann AP, Hambor JE, Grasser WA 3rd, Pan LC, Owen TA, Luzzio MJ, Hulford CA, Gebhard DF, Paralkar VM, Simmons HA, Kath JC, Roberts WG, Smock SL, Guzman-Perez A, Brown TA, Li M. Proline-rich tyrosine kinase 2 regulates osteoprogenitor cells and bone formation, and offers an anabolic treatment approach for osteoporosis. Proc Natl Acad Sci U S A. 2007; 104:10619–10624. [PubMed: 17537919]
35. Bajpai AK, Blaskova E, Pakala SB, Zhao T, Glasgow WC, Penn JS, Johnson DA, Rao GN. 15(S)-HETE production in human retinal microvascular endothelial cells by hypoxia: Novel role for MEK1 in 15(S)-HETE induced angiogenesis. Invest Ophthalmol Vis Sci. 2007; 48:4930–4938. [PubMed: 17962441]
36. Zhao T, Wang D, Cheranov SY, Karpurapu M, Chava KR, Kundumani-Sridharan V, Johnson DA, Penn JS, Rao GN. A novel role for activating transcription factor-2 in 15(S)-hydroxyeicosatetraenoic acid-induced angiogenesis. J Lipid Res. 2009; 50:521–533. [PubMed: 18849464]
37. Ross R. Atherosclerosis--an inflammatory disease. N Engl J Med. 1999; 340:115–126. [PubMed: 9887164]
38. Morgantini C, Imaizumi S, Grijalva V, Navab M, Fogelman AM, Reddy ST. Apolipoprotein A-I mimetic peptides prevent atherosclerosis development and reduce plaque inflammation in a murine model of diabetes. Diabetes. 2010; 59:3223–3228. [PubMed: 20826564]
39. Poeckel D, Zemski Berry KA, Murphy RC, Funk CD. Dual 12/15- and 5-lipoxygenase deficiency in macrophages alters arachidonic acid metabolism and attenuates peritonitis and atherosclerosis in ApoE knock-out mice. J Biol Chem. 2009; 284:21077–21089. [PubMed: 19509298]
40. Okigaki M, Davis C, Falasca M, Harroch S, Felsenfeld DP, Sheetz MP, Schlessinger J. Pyk2 regulates multiple signaling events crucial for macrophage morphology and migration. Proc Natl Acad Sci U S A. 2003; 100:10740–10745. [PubMed: 12960403]

41. Katsume A, Okigaki M, Matsui A, Che J, Adachi Y, Kishita E, Yamaguchi S, Ikeda K, Ueyama T, Matoba S, Yamada H, Matsubara H. Early inflammatory reactions in atherosclerosis are induced by proline-rich tyrosine kinase/reactive oxygen species-mediated release of tumor necrosis factor-alpha and subsequent activation of the p21Cip1/Ets-1/p300 system. Arterioscler Thromb Vasc Biol. 2011; 31:1084–1092. [PubMed: 21372295]
42. Andre P, Morooka T, Sim D, Abe K, Lowell C, Nanda N, Delaney S, Siu G, Yan Y, Hollenbach S, Pandey A, Gao H, Wang Y, Nakajima K, Parikh SA, Shi C, Phillips D, Owen W, Sinha U, Simon DI. Critical role for Syk in responses to vascular injury. Blood. 2011; 118:5000–5010. [PubMed: 21881044]
43. Gadepalli R, Singh NK, Kundumani-Sridharan V, Heckle MR, Rao GN. Novel role of proline-rich nonreceptor tyrosine kinase 2 in vascular wall remodeling after balloon injury. Arterioscler Thromb Vasc Biol. 2012; 32:2652–2661. [PubMed: 22922962]
44. Kyriakis JM, Avruch J. Mammalian MAPK signal transduction pathways activated by stress and inflammation: a 10-year update. Physiol Rev. 2012; 92:689–737. [PubMed: 22535895]
45. Altarejos JY, Montminy M. CREB and the CRTC co-activators: sensors for hormonal and metabolic signals. Nat Rev Mol Cell Biol. 2011; 12:141–151. [PubMed: 21346730]
46. Benito E, Barco A. CREB's control of intrinsic and synaptic plasticity: implications for CREB-dependent memory models. Trends Neurosci. 2010; 33:230–240. [PubMed: 20223527]
47. Khan BV, Parthasarathy SS, Alexander RW, Medford RM. Modified low density lipoprotein and its constituents augment cytokine-activated vascular cell adhesion molecule-1 gene expression in human vascular endothelial cells. J Clin Invest. 1995; 95:1262–1270. [PubMed: 7533787]
48. Huo Y, Zhao L, Hyman MC, Shashkin P, Harry BL, Burcin T, Forlow SB, Stark MA, Smith DF, Clarke S, Srinivasan S, Hedrick CC, Praticò D, Witztum JL, Nadler JL, Funk CD, Ley K. Critical role of macrophage 12/15-lipoxygenase for atherosclerosis in apolipoprotein E-deficient mice. Circulation. 2004; 110:2024–2031. [PubMed: 15451785]
49. Taleb S, Romain M, Ramkhelawon B, Uyttenhove C, Pasterkamp G, Herbin O, Esposito B, Perez N, Yasukawa H, Van Snick J, Yoshimura A, Tedgui A, Mallat Z. Loss of SOCS3 expression in T cells reveals a regulatory role for interleukin-17 in atherosclerosis. J Exp Med. 2009; 206:2067–2077. [PubMed: 19737863]
50. Smith E, Prasad KM, Butcher M, Dobrian A, Kolls JK, Ley K, Galkina E. Blockade of interleukin-17A results in reduced atherosclerosis in apolipoprotein E-deficient mice. Circulation. 2010; 121:1746–1755. [PubMed: 20368519]
51. Madhur MS, Funt SA, Li L, Vinh A, Chen W, Lob HE, Iwakura Y, Blinder Y, Rahman A, Quyyumi AA, Harrison DG. Role of interleukin 17 in inflammation, atherosclerosis, and vascular function in apolipoprotein e-deficient mice. Arterioscler Thromb Vasc Biol. 2011; 31:1565–1572. [PubMed: 21474820]
52. Fogh K, Larsen CG, Iversen L, Kragballe K. Interleukin-8 stimulates the formation of 15-hydroxy-eicosatetraenoic acid by human neutrophils in vitro. Agents Actions. 1992; 35:227–231. [PubMed: 1529797]
53. Zhang LH, Kamanna VS, Ganji SH, Xiong XM, Kashyap ML. Pioglitazone increases apolipoprotein A-I production by directly enhancing PPRE-dependent transcription in HepG2 cells. J Lipid Res. 2010; 51:2211–2222. [PubMed: 20371549]
54. Singh NK, Wang D, Kundumani-Sridharan V, Van Quyen D, Niu J, Rao GN. 15-Lipoxygenase-1-enhanced Src-Janus kinase 2-signal transducer and activator of transcription 3 stimulation and monocyte chemoattractant protein-1 expression require redox-sensitive activation of epidermal growth factor receptor in vascular wall remodeling. J Biol Chem. 2011; 286:22478–22488. [PubMed: 21536676]
55. Tian XY, Wong WT, Xu A, Lu Y, Zhang Y, Wang L, Cheang WS, Wang Y, Yao X, Huang Y. Uncoupling protein-2 protects endothelial function in diet-induced obese mice. Circ Res. 2012; 110:1211–1216. [PubMed: 22461387]

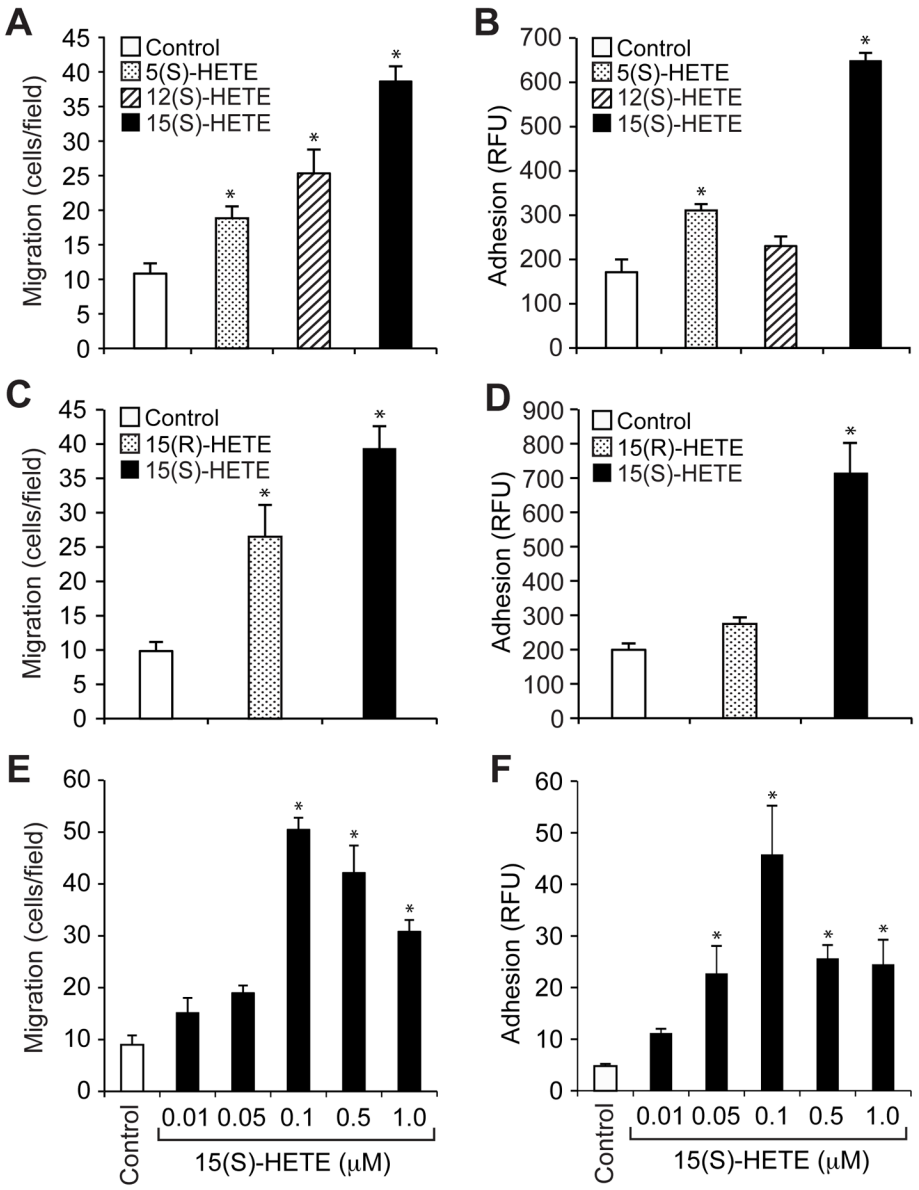

Fig 1. 15(S)-HETE stimulates the migration and adhesion of THP1 cells

(**A** to **D**) Effects of various HETEs on the migration and adhesion of THP1 cells. (A and C) The migration of THP1 cells in response to vehicle (Control) or the indicated HETE (0.1 μM) was measured by the modified Boyden chamber method. (B and D) Quiescent THP1 cells were treated with vehicle (Control) or the indicated HETE (0.1 μM) for 1 hour, labeled with 10 μM BCECF-AM for 30 min, overlaid onto a monolayer of quiescent HUVECs, and incubated for 2 hours. Adherent cells were determined by measuring fluorescence intensity. (**E** and **F**) The migration and adhesion of THP1 cells were measured as described for (A) to (D) in response to the indicated doses of 15(S)-HETE. Data are means ± SD from three independent experiments. **P* < 0.01 versus control.

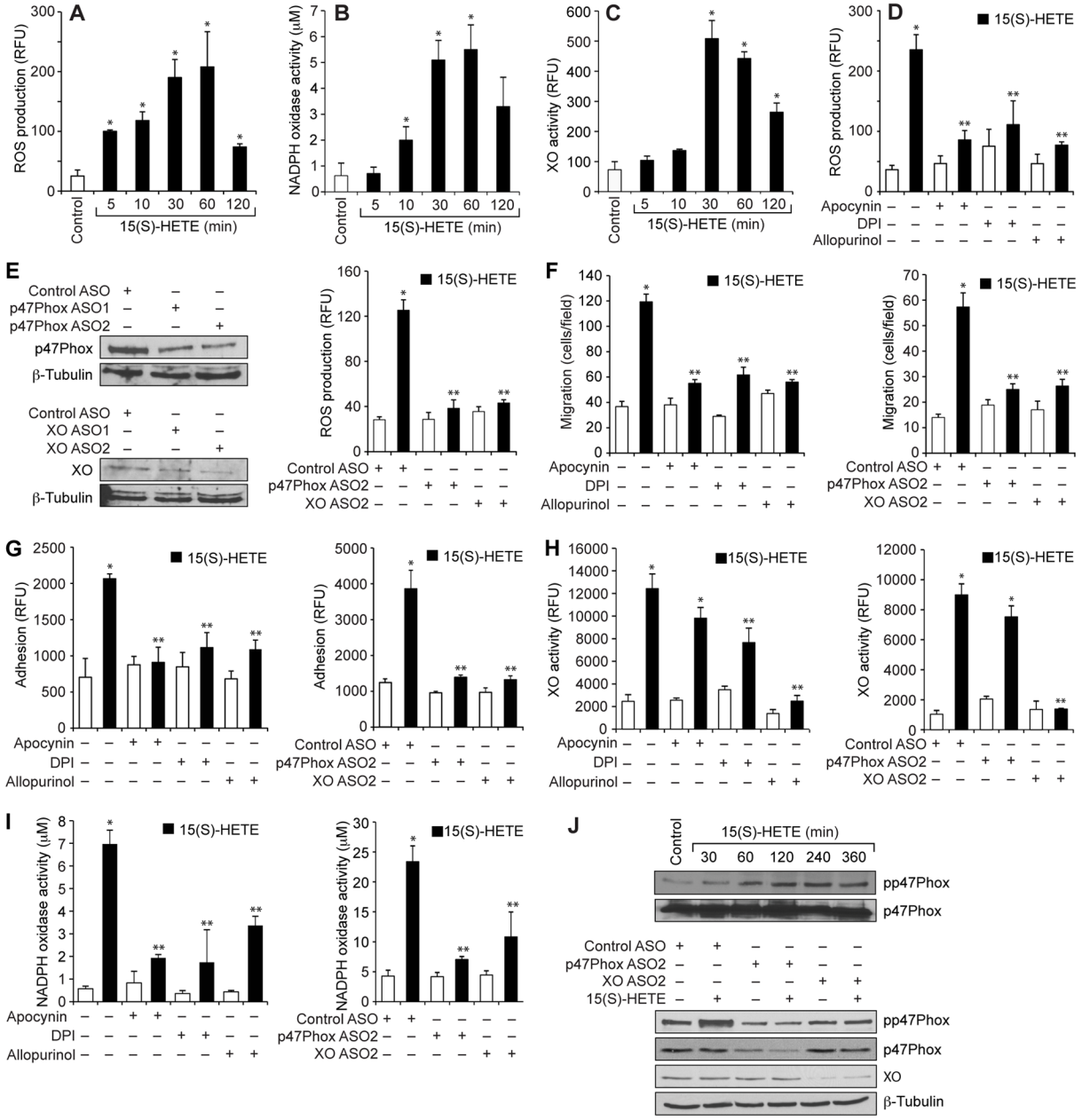

Fig 2. The 15(S)-HETE–stimulated migration and adhesion of THP1 cells require ROS production

(**A** to **D**) THP1 cells were treated with (A to C) vehicle (Control) or 0.1 μM 15(S)-HETE for the indicated times or with (D) vehicle (Control) or 0.1 μM 15(S)-HETE in the absence or presence of 100 μM apocynin, 10 μM DPI, or 100 μM allopurinol for 1 hour. (A and D) ROS production, (B) NADPH oxidase activity, and (C) xanthine oxidase (XO) activity were measured. (**E**) Left: THP1 cells were transfected with control, p47Phox-specific, or XO-specific ASOs (100 nM). Forty-eight hours later, the abundances of p47Phox and XO were analyzed by Western blotting and were normalized to that of β-tubulin. Right: Forty-eight hours after transfection, quiescent cells were treated with vehicle or 0.1 μM 15(S)-HETE for 1 hour before being analyzed for ROS production. (**F** to **I**) Left panels: THP1 cells were treated with vehicle (empty bars) or 0.1 μM 15(S)-HETE (filled bars) in the presence or

absence of the indicated inhibitors before being analyzed for (F) migration, (G) adhesion, (H) XO activity, and (I) NADPH oxidase activity. Right panels: THP1 cells transfected with control ASO or the indicated ASOs were treated with vehicle (empty bars) or 0.1 μM 15(S)-HETE (filled bars) before being analyzed for (F) migration, (G) adhesion, (H) XO activity, and (I) NADPH oxidase activity. (**J**) Top: Whole-cell lysates of vehicle-treated THP1 cells or THP1 cells that were treated with 0.1 μM 15(S)-HETE for the indicated times were analyzed by Western blotting with antibodies against the indicated proteins. Bottom: THP1 cells were transfected with the indicated ASOs and allowed to rest before being treated with 15(S)-HETE for 1 hour and then were analyzed by Western blotting with antibodies against the indicated proteins. Data in (A) to (I) are means ± SD from three independent experiments. *$P < 0.01$ versus control; **$P < 0.01$ versus 15(S)-HETE. Western blots in (J) are from one experiment and are representative of three independent experiments.

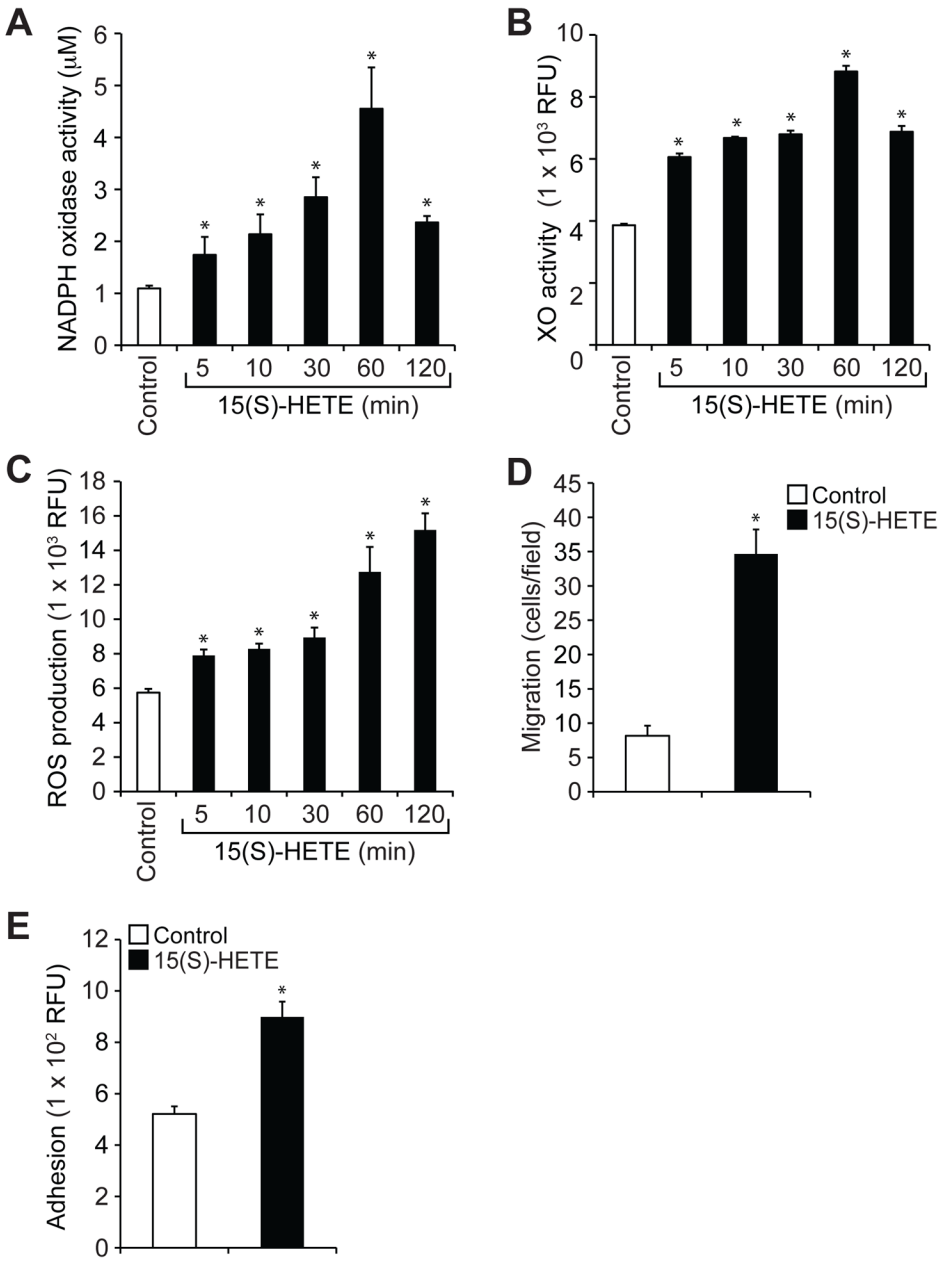

Fig 3. 15(S)-HETE stimulates NADPH oxidase and xanthine oxidase activities and ROS production in mouse peritoneal macrophages and enhances their migration and adhesion

(**A** to **C**) Quiescent mouse peritoneal macrophages were treated with vehicle (Control) or 0.1 μM 15(S)-HETE for the indicated times before being analyzed for (A) NADPH oxidase activity, (B) XO activity, and (C) ROS production. (**D**) The migration of quiescent macrophages in response to vehicle (Control) or 0.1 μM 15(S)-HETE was measured by the modified Boyden chamber method. (**E**) Quiescent macrophages were treated with vehicle (Control) or 0.1 μM 15(S)-HETE for 1 hour, labeled with 10 μM BCECF-AM for 30 min, overlaid onto a monolayer of quiescent mouse endothelial cells, and incubated for 2 hours. Adherent cells were determined by measuring fluorescence intensities. Data are means ± SD from three independent experiments. **P* < 0.01 versus control.

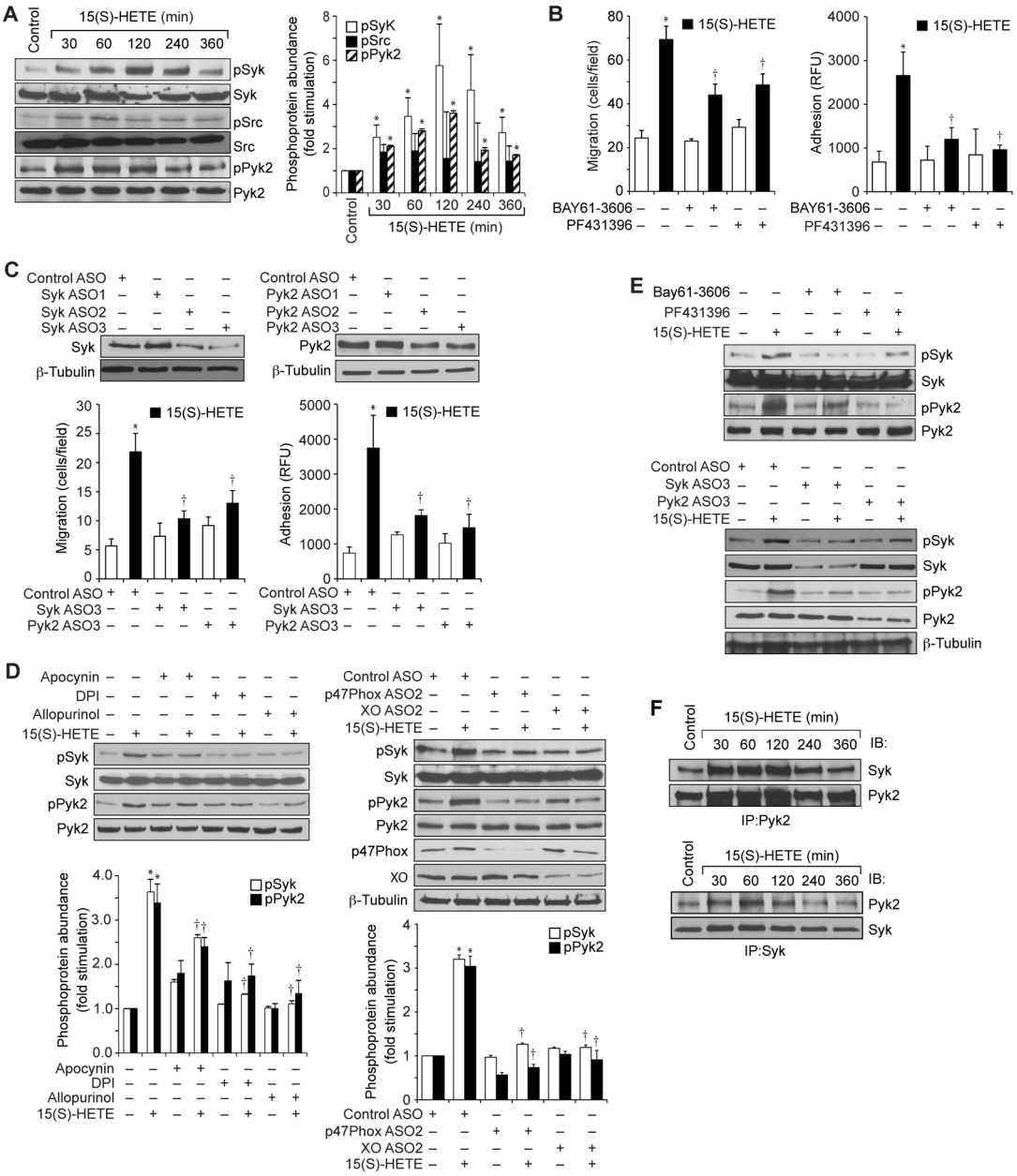

Fig 4. Syk and Pyk2 mediate the 15(S)-HETE–dependent migration and adhesion of THP1 cells

(**A**) Whole-cell lysates of vehicle-treated THP1 cells or of cells treated with 0.1 μM 15(S)-HETE for the indicated times were analyzed by Western blotting with antibodies against the indicated proteins. Bar graph shows densitometric analysis of the fold-increase in the abundance of pSyk, pSrc and pPyk2 at the indicated times of 15(S)-HETE treatment compared to that in vehicle-treated cells. (**B**) THP1 cells were pretreated with vehicle, 10 μM BAY61-3606, or 5 μM PF431396 for 30 min before being treated with 0.1 μM 15(S)-HETE and then analyzed for migration (left) and adhesion (right) as described earlier. (**C**) Top: Western blotting analysis of the effects of Syk- and Pyk2-specific ASOs on their targets. Bottom: THP1 cells transfected with the indicated ASOs and allowed to rest were treated with vehicle or 0.1 μM 15(S)-HETE before being analyzed for migration and adhesion. (**D**) Left: THP1 cells were treated with vehicle or 0.1 μM 15(S)-HETE in the

absence or presence of the indicated inhibitors for 1 hour and then were analyzed by Western blotting with antibodies specific for the indicated proteins. Right: THP1 cells transfected with the indicated ASOs were allowed to rest before being treated with vehicle or 0.1 μM 15(S)-HETE for 1 hour and then were analyzed by Western blotting with antibodies against the indicated proteins. Bar graph shows densitometric analysis of the fold-increase in the abundance of pSyk and pPyk2 for each condition compared to that in vehicle-treated cells. (**E**) Inhibition or knockdown of Syk or Pyk2 reciprocally affects their 15(S)-HETE–dependent phosphorylation. THP1 cells treated with the indicated inhibitors (top) or transfected with the indicated ASOs (bottom) were treated with vehicle or 0.1 μM 15(S)-HETE before being analyzed by Western blotting with antibodies against the indicated proteins. (**F**) THP1 cells treated with vehicle (Control) or with 0.1 μM 15(S)-HETE for the indicated times were subjected to immunoprecipitation (IP) with anti-Pyk2 or anti-Syk antibodies, and the immunoprecipitates were analyzed by Western blotting (IB) with antibodies specific for Syk or Pyk2. Data in (A) to (D) are means ± SD from three independent experiments. $^{*}P < 0.01$ versus control; $^{\dagger}P < 0.01$ versus 15(S)-HETE. Western blots are from one experiment and are representative of three independent experiments.

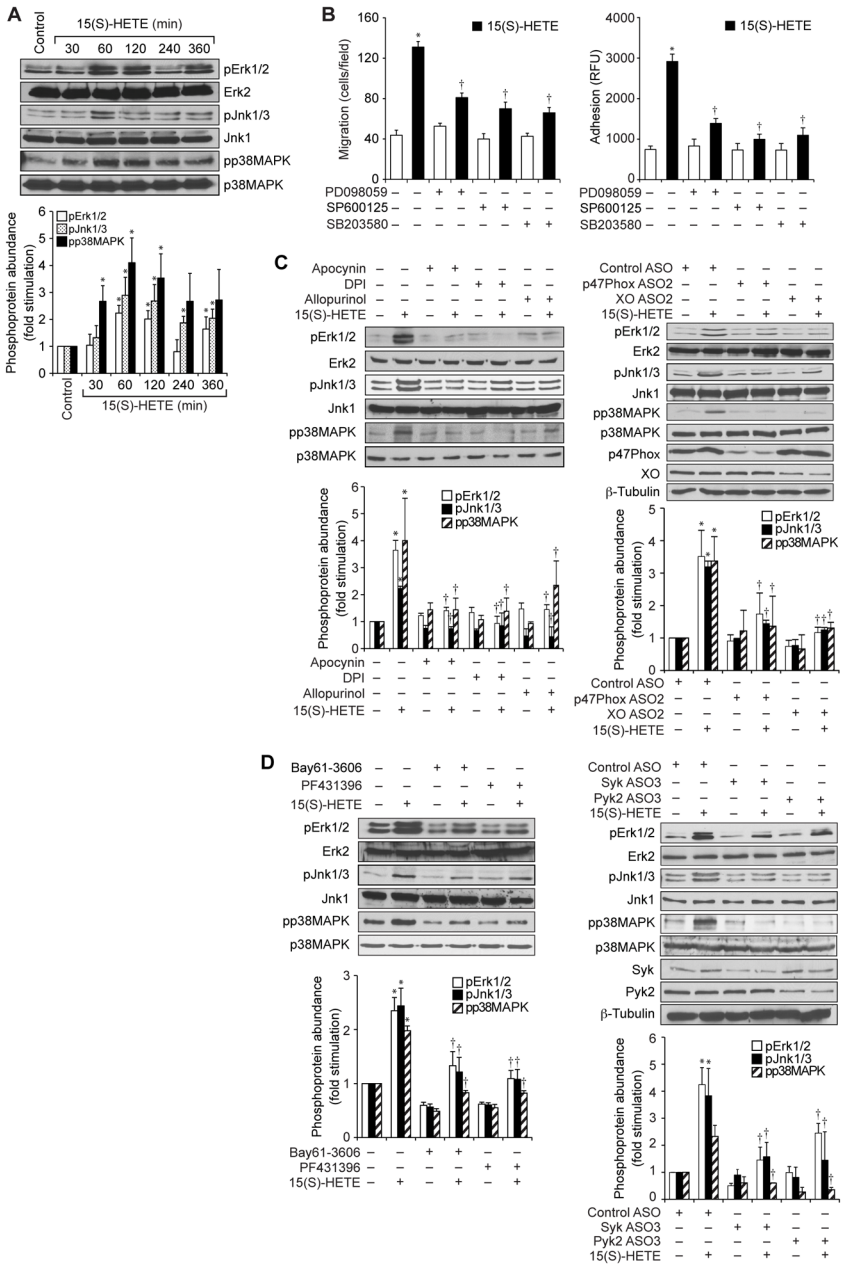

Fig 5. MAPKs mediate the 15(S)-HETE–dependent migration and adhesion of THP1 cells

(**A**) Whole-cell lysates of vehicle-treated THP1 cells (Control) or of THP1 cells treated with 0.1 μM 15(S)-HETE for the indicated times were analyzed by Western blotting with antibodies specific for the indicated proteins. Bar graph shows densitometric analysis of the fold-increase in the abundance of pErk1/2, pJnk1/3 and pp38MAPK at the indicated times of 15(S)-HETE treatment compared to that in vehicle-treated cells. (**B**) THP1 cells were pretreated for 30 min with vehicle, 30 μM PD098059, 10 μM SP600125, or 10 μM SB203580 before being treated with vehicle or 0.1 μM 15(S)-HETE and then being analyzed for migration (left) and adhesion (right). (**C** and **D**) THP1 cells were treated with the indicated inhibitors or were transfected with the indicated ASOs before being treated with vehicle or 0.1 μM 15(S)-HETE for 1 hour. Whole-cell lysates were then analyzed by Western blotting with antibodies specific for the total and phosphorylated forms of the

indicated MAPK proteins, p47Phox, XO, Syk, and Pyk2. β-tubulin was used as a loading control. Bar graph shows densitometric analysis of the fold-increase in the abundance of pErk1/2, pJnk1/3 and pp38MAPK for each condition compared to that in vehicle-treated cells. Western blots are from one experiment and are representative of three independent experiments. Data in bar graphs are means ± SD from three independent experiments. *$P <$ 0.01 versus control; $^{\dagger}P < 0.01$ versus 15(S)-HETE.

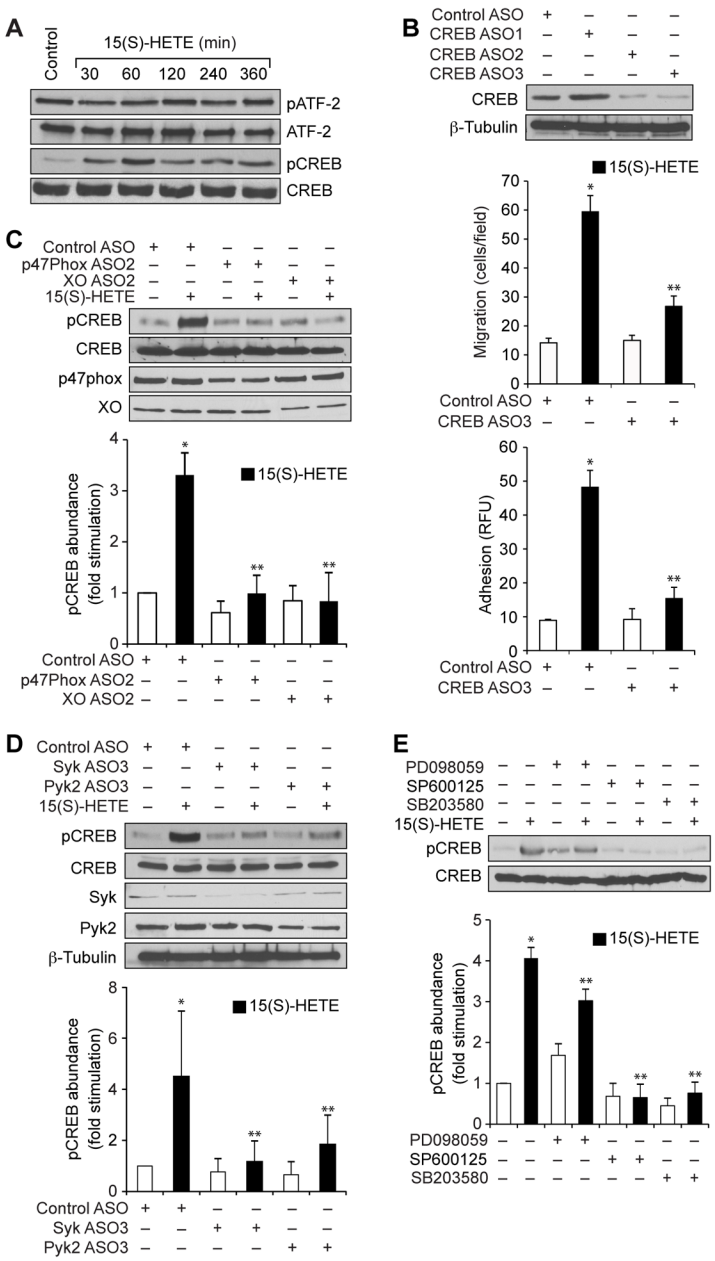

Fig 6. CREB mediates the 15(S)-HETE–dependent migration and adhesion of THP1 cells

(**A**) Whole-cell lysates of vehicle-treated THP1 cells or of THP1 cells treated with 0.1 μM 15(S)-HETE for the indicated times were analyzed by Western blotting with antibodies against the indicated proteins. (**B**) THP1 cells transfected with control ASO or CREB-specific ASOs were treated with vehicle or 0.1 μM 15(S)-HETE for 1 hour before undergoing Western blotting analysis with antibodies against the indicated proteins (top), or being analyzed for migration (middle) or adhesion (bottom). (**C** and **D**) THP1 cells transfected with control ASO or with ASOs specific for (C) the indicated oxidases or (D) the indicated kinases were allowed to rest after transfection before they were treated with vehicle or 0.1 μM 15(S)-HETE for 1 hour. Whole-cell lysates were analyzed by Western blotting with antibodies specific for the indicated proteins. Bar graph shows densitometric analysis of the fold-increase in the abundance of pCREB normalized to that of total CREB

for each condition compared to that in vehicle-treated cells transfected with control ASO. (**E**) THP1 cells were treated with vehicle or 0.1 μM 15(S)-HETE in the absence or presence of the indicated inhibitors for 1 hour before being analyzed by Western blotting with antibodies against the indicated proteins. Bar graph shows densitometric analysis of the fold-increase in the abundance of pCREB normalized to that of total CREB for each condition compared to that in vehicle-treated cells. Western blots are from one experiment and are representative of three independent experiments. Data in bar graphs are means ± SD from three independent experiments.*$P < 0.01$ versus control; **$P < 0.01$ versus 15(S)-HETE.

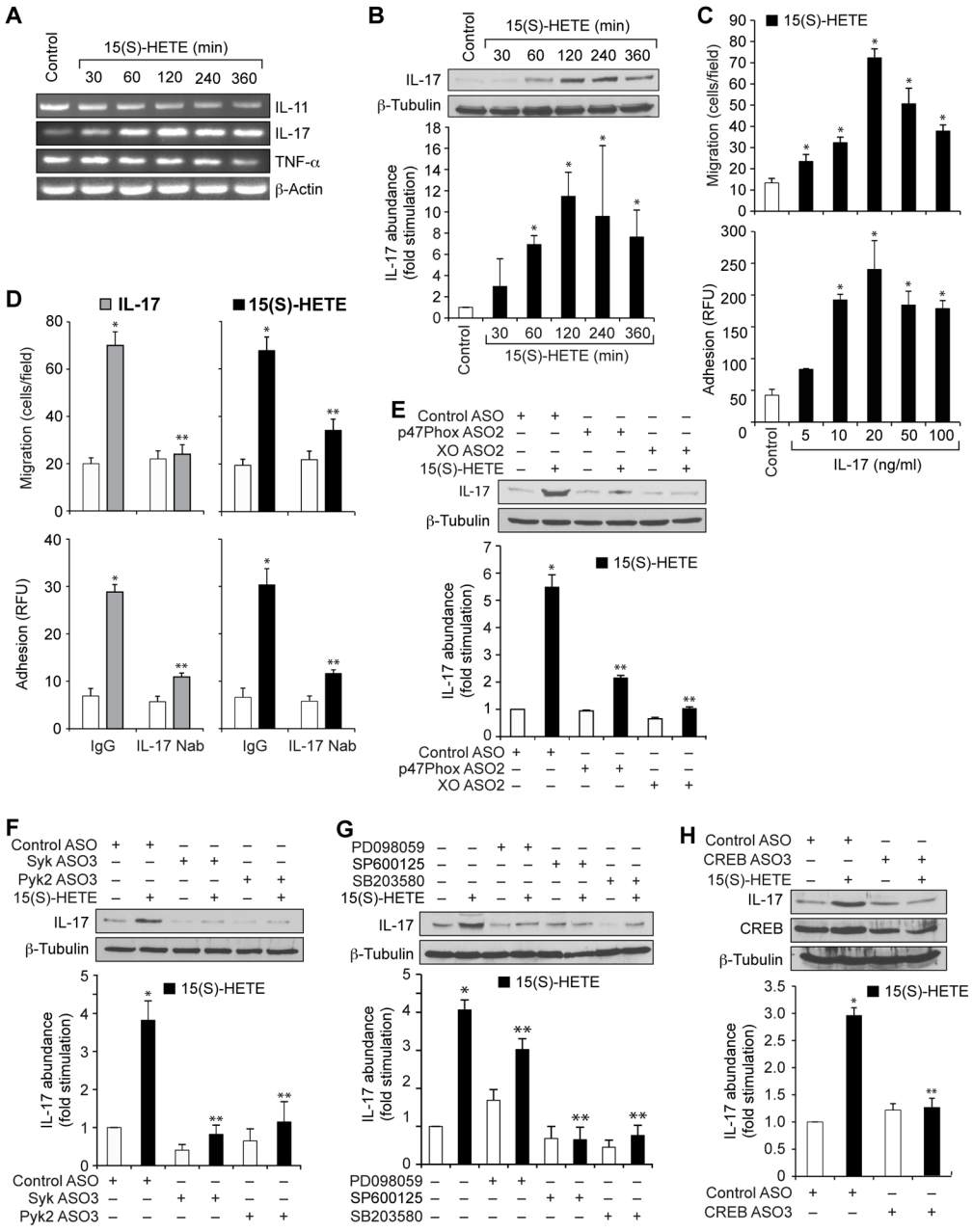

Fig 7. IL-17A mediates the 15(S)-HETE–stimulated migration and adhesion of THP1 cells

(**A**) THP1 cells were treated with vehicle or 0.1 μM 15(S)-HETE for the indicated times and then were analyzed by RT-PCR to determine the abundances of mRNAs for IL-11, IL-17, TNF-α, and β-actin. (**B**) Whole-cell lysates of vehicle-treated THP1 cells or of THP1 cells treated with 0.1 μM 15(S)-HETE for the indicated times were analyzed by Western blotting to determine the abundance of IL-17 protein. Bar graph shows densitometric analysis of the fold-increase in the abundance of IL-17 protein normalized to that of β-tubulin for the indicated times of 15(S)-HETE treatment compared to that in vehicle-treated cells. (**C**) THP1 cells were treated with vehicle (Control) or the indicated concentrations of IL-17A before being analyzed for migration (top) and adhesion (bottom). (**D**) THP1 cells were pretreated with normal immunoglobulin G (IgG) or neutralizing antibody (Nab) against

IL-17A before being treated with IL-17A (20 ng/ml, left) or 0.1 μM 15(S)-HETE (right) and then being analyzed for migration (top) or adhesion (bottom). (**E** and **F**) THP1 cells were transfected with control ASO or with ASOs specific for (E) the indicated oxidases or (F) the indicated kinases before being rested and then treated with vehicle or 15(S)-HETE for 2 hours. Whole-cell lysates were then analyzed by Western blotting with antibodies against the indicated proteins. Bar graphs show densitometric analysis of the fold-increase in the abundance of IL-17 protein normalized to that of β-tubulin for each condition compared to that in vehicle-treated cells transfected with control ASO. (**G**) THP1 cells were treated with vehicle or 0.1 μM 15(S)-HETE in the absence or presence of the indicated inhibitors for 2 hours before being analyzed by Western blotting with antibodies against the indicated proteins. Bar graph shows densitometric analysis of the fold-increase in the abundance of IL-17 protein normalized to that of β-tubulin for each condition compared to that in vehicle-treated cells. (**H**) THP1 cells were transfected with control or CREB-specific ASOs, rested, and then treated with vehicle or 0.1 μM 15(S)-HETE for 2 hours before being analyzed by Western blotting with antibodies against the indicated proteins. Bar graph shows densitometric analysis of the fold-increase in the abundance of IL-17 protein normalized to that of β-tubulin for each condition compared to that in vehicle-treated cells transfected with control ASO. Western blots are from one experiment and are representative of three independent experiments. Data in bar graphs are means ± SD from three independent experiments.*$P < 0.01$ versus control; **$P < 0.01$ versus 15(S)-HETE.

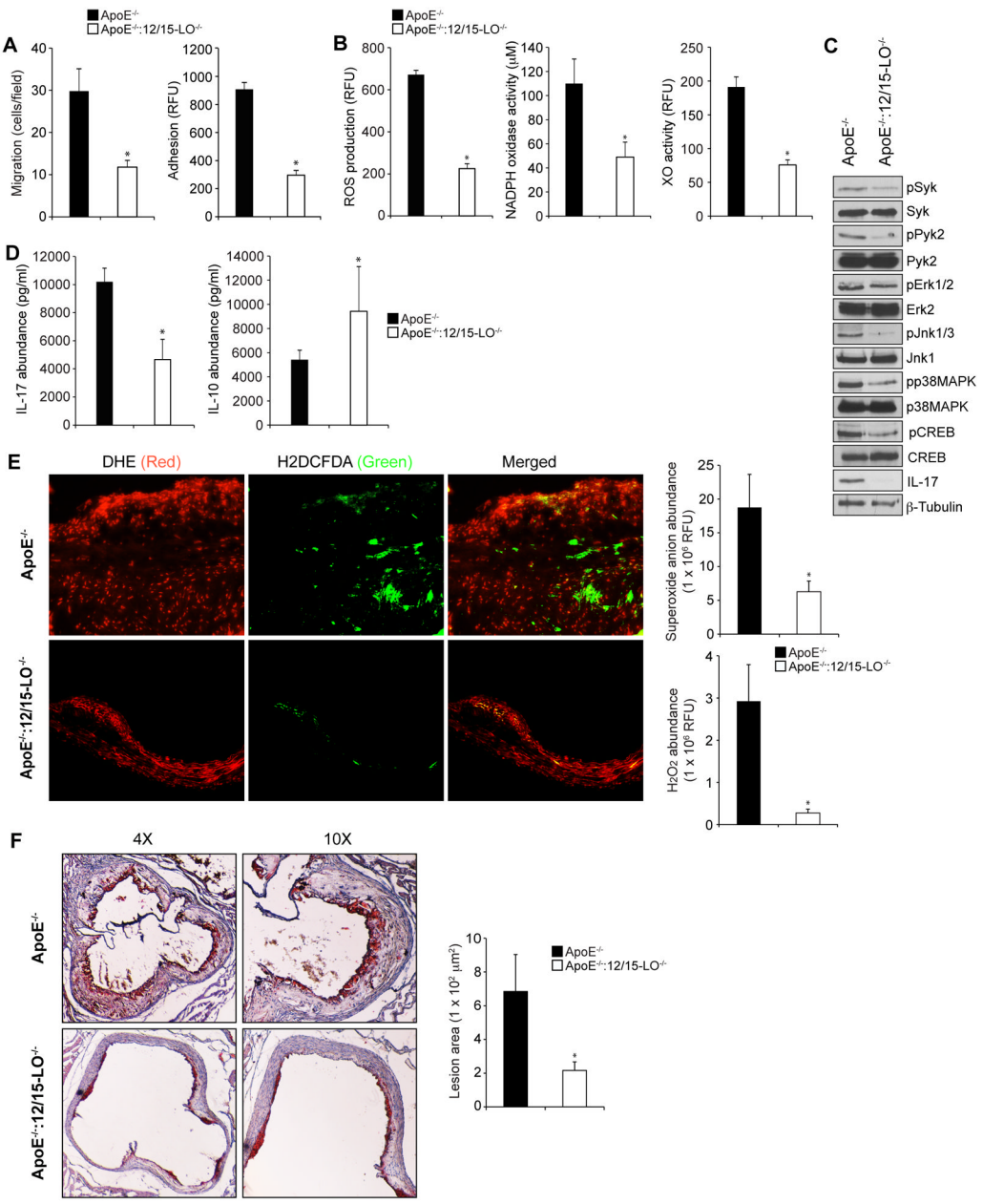

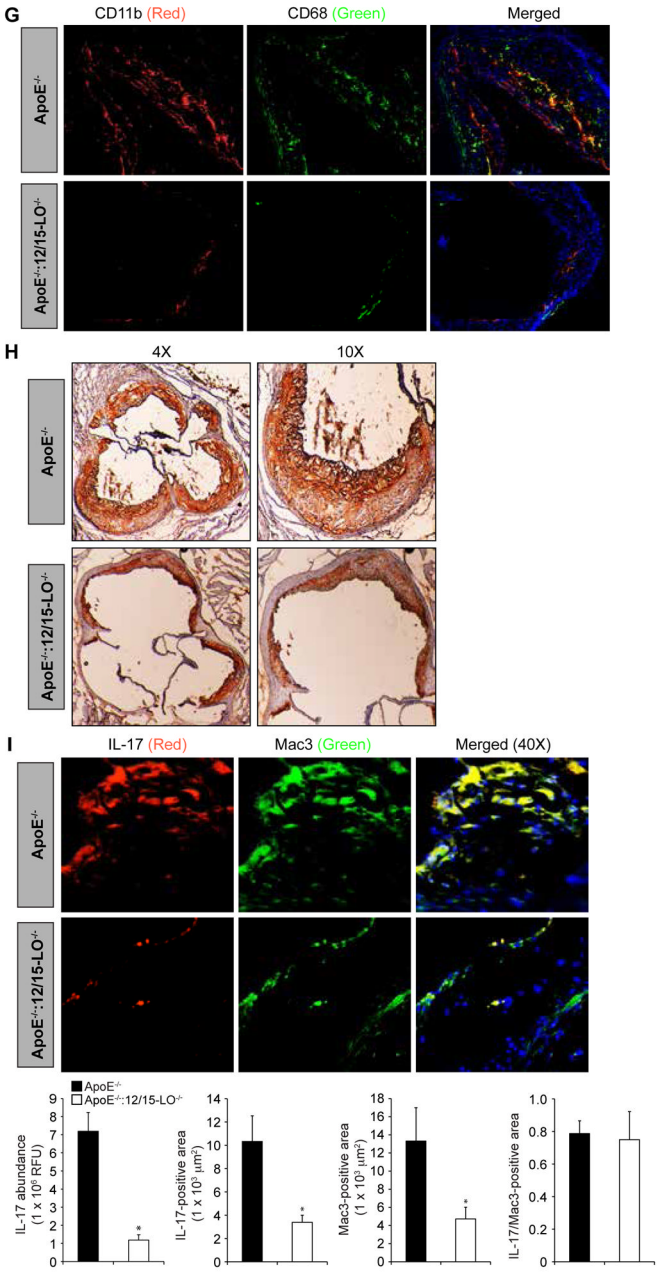

Fig 8. Loss of 12/15-LO inhibits diet-induced, CREB-dependent IL-17A production in macrophages, and attenuates their migration and adhesion

(**A** and **B**) ApoE$^{-/-}$ mice and ApoE$^{-/-}$:12/15-LO$^{-/-}$ mice were fed a high-fat diet for 8 weeks. Peritoneal macrophages were then isolated and were subjected to (A) migration and adhesion assays or (B) were lysed and assayed for ROS production, NADPH oxidase activity, and XO activity. (**C**) Whole-cell lysates of peritoneal macrophages isolated from the indicated mice described in (A) were analyzed by Western blotting with antibodies specific for the indicated proteins. β-tubulin was used as a loading control. (**D**) IL-17A and IL-10 concentrations in the plasma of the indicated mice described in (A) were measured by ELISA. (**E**) ROS abundances in atherosclerotic lesions were determined by staining cryosections of aortic roots isolated from the indicated mice described in (A) with DHE (to detect the superoxide anion) and H2DCFDA (to detect H_2O_2) and measuring fluorescence

intensities. The left panel shows images of the sections and the right panels show pooled data based on the fluorescence intensities. (**F**) Atherosclerotic lesions were assessed by Oil Red O-staining of cryosections of the aortic roots isolated from the indicated mice described in (A) and measuring the lesion areas. The left panel shows images of the sections and the right panel shows pooled data based on the staining intensities. (**G**) The extent of recruitment of monocytes in atherosclerotic lesions were examined by immunofluorescence staining of the cryosections described in (E) for CD11b and CD68. (H) The recruitment of macrophages in atherosclerotic lesions were examined by immunostaining of the cryosections described in (E) for Mac3. (**I**) Double immunofluorescence staining of the cryosections described in (E) for IL-17A (red) and Mac3 (green). The bar-graphs represent IL-17A abundance in the lesion, IL-17A-positive area in the lesion, Mac3-positive area in the lesion and the lesion area positive for both IL-17A and Mac3 in high-fat diet-fed $ApoE^{-/-}$ and $ApoE^{-/-}$:12/15-$LO^{-/-}$ mice. *$P < 0.01$ versus $ApoE^{-/-}$ mice (n = 6 mice per group).